DOCTORAL SCHOOL
UNIVERSITA' *MEDITERRANEA* DI REGGIO CALABRIA

DIPARTIMENTO DI INGEGNERIA DELL'INFORMAZIONE, DELLE INFRASTRUTTURE E DELL'ENERGIA SOSTENIBILE (DIIES)

PHD IN
INFORMATION ENGINEERING

S.S.D. ING-INF/02
XXXI CICLO

NOVEL PARADIGMS IN 3D FIELD INTENSITY SHAPING AND THEIR APPLICATION TO HYPERTHERMIA TREATMENT PLANNING

CANDIDATE
Gennaro BELLIZZI
[redacted]

ADVISOR
Prof. Tommaso ISERNIA
[redacted]

Co-ADVISOR
Dr. Lorenzo CROCCO
[redacted]

COORDINATOR
Prof. Tommaso ISERNIA
[redacted]

REGGIO CALABRIA, FEBBRAIO 2019

Finito di stampare nel mese di **Febbraio 2019**

Edizione CSdA Centro Stampa d'Ateneo

Quaderno N. 38
Collana *Quaderni del Dottorato di Ricerca in Ingegneria dell'Informazione*
Curatore *Prof. Tommaso Isernia*

ISBN 978-88-99352-25-7

Università degli Studi *Mediterranea* di Reggio Calabria
Salita Melissari, Feo di Vito, Reggio Calabria

GENNARO BELLIZZI

NOVEL PARADIGMS IN 3D FIELD INTENSITY SHAPING AND THEIR APPLICATION TO HYPERTHERMIA TREATMENT PLANNING

The Teaching Staff of the PhD course in
INFORMATION ENGINEERING
consists of:

Tommaso ISERNIA (Coordinatore)
Pierluigi ANTONUCCI
Giovanni ANGIULLI
Giuseppe ARANITI
Francesco BUCCAFURRI
Rosario CARBONE
Riccardo CAROTENUTO
Salvatore COCO
Maria Antonia COTRONEI
Claudio DE CAPUA
Francesco DELLA CORTE
Aimè LAY EKUAKILLE
Pasquale G. F. FILIANOTI
Patrizia FRONTERA
Sofia GIUFFRÈ
Antonio IERA
Gianluca LAX
Giacomo MESSINA
Antonella MOLINARI
Andrea F. MORABITO
Rosario MORELLO
Fortunato PEZZIMENTI
Sandro RAO
Domenico ROSACI
Giuseppe RUGGERI
Maria Teresa RUSSO
Valerio SCORDAMAGLIA
Domenico URSINO

And also:
Antoine BERTHET
Dominique DALLET
Lubomir DOBOS
Lorenzo CROCCO
Ivo RENDINA
Groza VOICU

Dedicata a mio fratello, Giovanni

Zwei Dinge sollten Kinder von ihren Eltern bekommen: Wurzeln und Flügel[1]

— J. W. v. Goethe, 1749 - 1832

Acknowledgments

As first, I would like to express my gratitude to my advisor, Professor Tommaso Isernia, for the continuous support, for his patience, motivation and his immense knowledge. His guidance and his tuition taught me in loving this job. I could not have asked for a better advisor and mentor. In particular, I am grateful to Professor Isernia for have pushed and warned me in many occasions. Finally, I will never forget the great experience of being part of the "Big Brother House" as well as the many hours of driving together.

My sincere thanks goes to Dr. Lorenzo Crocco, my co-advisor and friend. His high scientific guidance and his strong and large international networking provided me with invaluable opportunities which broadened my mind and my view of the world. Moreover, I am thankful to Dr. Crocco because he was the first who believed in me since my bachelor thesis. Without his precious support, nothing of this would have been possible.

Thanks to Professor Maarten Paulides. I appreciated and enjoyed all the discussions we had and I look forward the many we have ahead. I thank Professor Paulides for the trust and for the many opportunities he provided me with. I hope to treasure all of it to the best. Finally, I thank Professor Paulides for having me into his home: this is even more valuable to me than the rest.

I am very thankful to Professor Gerard van Rhoon for his insightful teaching and encouragement, but also for all the discussions we had, both professional and non-professional. I am really grateful to Professor van Rhoon for the care he has to me.

[1] Translation — Two things children should receive from their parents: roots and wings.

Traduzione — Due cose i bambini dovrebbero ricevere dai propri genitori: Radici e Ali

Thanks to Martina Bevacqua, Rosa Scapaticci, Kemal Sümser, Andrea Morabito, Roberta Palmeri and Giada Battaglia. They always encouraged and helped me during these years. I am very thankful to all of them for the warmth with which they accepted me. I look forward many years of joint works.

Ogni passo che faccio, ogni giorno che vivo, questo dottorato così come ogni altra cosa nella mia vita non sarebbe nulla senza mio fratello Giovanni. Il tuo vivere ed il tuo pensare mi ha insegnato tanto. Questa tesi, così come ogni soddisfazione e/o vittoria è comune: quindi anche quest'altra piccola bandierina è nostra. La strada da fare sarà sempre tanta, ma insieme la vivremo sempre a testa alta e con il sorriso.

Grazie a Mamma e Papà. Grazie perchè siete e sarete sempre la mia forza. Grazie per avermi dato più di quanto avevo bisogno, sempre. Grazie perchè mi avete insegnato che questo dottorato non vale niente se non si è felici. Grazie per avermi reso **FELICE**. Mi avete dato radici, per sapere da dove vengo, ed ali, per volare e vivere il mondo. Questo mi ha dato e mi darà sempre la possibilità di sperimentare, vivere, vincere e fallire sapendo di poter sempre tornare a casa.

Grazie ai **NoCromatiOccasionali**: i miei amici! Quelli veri, quelli che ci sono sempre stati per me. La nostra amicizia è nata, è cresciuta ed è maturata legandoci sempre di più. Sono sicuro che con gli anni riusciremo a riunirci di nuovo in una città per poterci vivere ogni giorno. Siete stati e sarete il mio sorriso!

Grazie a Marti, Max, Cosim8 e La Dottoressa Bevacqua. Amici e in teoria anche colleghi. Ho nel cuore ogni momento insieme, il marmo a casa di Max, ogni passeggiata, granita e risata. Senza voi lasciare Reggio Calabria sarebbe stato molto più facile.

Grazie agli **Uovini Nuomi**. Siete stati e siete un turbinio di emozioni nato da un incontro ed entratomi nel cuore e nella mente. Grazie per tutte le risate, gli insulti, le grandi mangiate e grazie per avermi fatto sentire a casa anche se lontano da Napoli. Vivere a Reggio, grazie a voi, era naturale, bello e mi manca, così come mi mancate voi. In particolare, grazie a Rudy, per avermi aperto le porte di casa sua, per aver creduto nella nostra Amicizia e nella possibilità di progettare insieme. Grazie a tutta la sua famiglia per avermi trattato come un nipote.

Grazie assaje,

Gennaro

Abstract

The problem of shaping the intensity distribution of an electromagnetic field is a canonical and fundamental problem of wave physics, which is relevant to many applications ranging from telecommunications, biomedical engineering and energy harvesting. In this framework, this thesis introduces novel paradigms for the field intensity shaping and deals with their applications to the hyperthermia treatment planning.

Hyperthermia is a cancer treatment modality in which the tumor temperature is elevated to a supra-physiologic temperature (40–44°C) for 60-90min. Clinical trials have demonstrated the therapeutic benefit of this treatment in combination with radio- and chemo-therapy. According to the clinical findings, further increase of temperature would enhance the clinical effectiveness. In this respect, further progress and widespread clinical adoption of hyperthermia are dependent on the development of accurate treatment optimization approaches able to sharply control the administered heating. Optimization of the heating pattern is nowadays tackled by optimally determining the complex excitation coefficients feeding a phased array applicator.

In the thesis, the problem of inducing a homogeneous temperature over a given target area while avoiding high temperatures in healthy tissues has been faced. In particular, different hyperthermia treatment planning optimization approaches have been proposed and clinically tested. For the first time, the multi-objective non-convex problem of maximizing the power deposition within a given target volume constraining it to prescribed level outside has been tackled by means of a convex optimization problem.

The achieved clinical results suggested that the nowadays clinically adopted optimization approaches are not able to successfully deal with the locally advanced tumors (i.e., the larger target volumes). In other words, "just" focusing the power deposition distribution in a target point set into such a target volume was shown to be a sub-optimal solution for such challenging cases where a shaped distribution is needed. Hence, the novel paradigm of power deposition shaping (as opposed to power deposition focusing) has been herein introduced and novel shaping optimization approaches have been developed and tested.

Contents

List of Figures

List of Tables

I

Introduction

Shaping a wavefield (acoustic or electromagnetic) into an inhomogeneous medium is a challenging as well as an open problem in applied physics. Besides the methodological point of view, this is relevant in many applications where there is the need of conveying the energy carried by the wavefield in a desired space location while taking into account interactions with the surrounding environment.

The range of application spans from telecommunications to geophysical prospecting, non-destructive testing and medicine [1–7]. Concerning geophysical prospecting, the problem is that of efficiently detecting buried targets. Analogously, the same problem is that of probing earthquake epicenters [3]. In the telecommunications, this problem plays a crucial role in the propagation of waves into complex environments (e.g., in urban scenarios) as well as it is useful to reduce channel dispersion and interference in wireless communications [8].

Analogously, a properly shaped wavefield results to be of particular relevance in different medical-related applications such as MRI shimming, High-Intensity Focused Ultrasound (HIFU), Extracorporeal Shock Wave Lithotripsy (ESWL) and hyperthermia [5, 6, 9, 10]. As an example, HIFU aims at generating very high temperatures (up to 100°C) through focused/shaped ultrasound fields to perform a very precise non-invasive tissue heating (mild hyperthermia or ablation). Another noteworthy example is ESWL. This aims at focusing the acoustic pressure field in order to non-invasively disintegrating kidney stones. Although similar in spirit, no thermal effects are exploited here. Finally, a clinically challenging and interesting application is represented by hyperthermia. This is a cancer treatment adjuvant modality based on the selective cancer temperature increase achieved through properly shaping the power deposition.

A common point to all the aforementioned applications is the need of a strategy to properly drive (i.e., phase and amplitude) a given phased array applicator in order to generate the desired power shaping. In this framework, the innovative contribute of this thesis is that of proposing novel optimization strategies for the “optimal” shaping

of a wavefield (ultrasound or electromagnetic). Besides the interest in the methodology, this thesis deals specifically with the relevant problem of planning a hyperthermia treatment. In collaboration with the *Hyperthermia Unit of the Department of Radiation Oncology at the Erasmus MC* (Rotterdam, The Netherlands), the proposed strategies have been clinically tested and comparatively assessed on actual patient data. The clinical assessment have been pursued within the very challenging clinical scenario of patients with head & neck (H&N) cancer. This scenario presents a very good case for assessment of the benefit of novel shaping approaches. In fact, target conformal heating is possible and therefore the optimal planning of the treatment is pivotal and routinely used [5]. Therefore, this scenario is highly suited for our aims in terms of predicted treatment quality and computational costs.

A description of the problem of hyperthermia is given in Chapter 1. Firstly, the different approaches proposed in the literature are reviewed. Secondly, without loss of generality the clinical hyperthermia workflow is given with some specific hints to the H&N, being this the site chosen for comparison. Thirdly, the shaping approach adopted at Erasmus MC, as presented in [11], has been detailed described both to provide an example from the state-of-the-art and to provide details on the approach adopted in the following comparison. Finally, the structure of the thesis is given only at the end of Chapter 1 since, despite the broad range of applicability, the proposed approaches have been developed starting from specific clinical needs, hence better framed after the description of the problem.

1

A Promising Thermal Therapy: Hyperthermia

Hyperthermia belongs to the class of thermal cancer treatments. It consists in a selective increase of the tumor temperature to a supra-physiologic temperature ($40-44°C$) for 60-90min. Clinical trials have demonstrated the therapeutic benefit of this treatment in combination with radio- and chemo-therapy [12–15]. Given the thermal dose-effect relations found in literature [13, 16], selective increase of the temperature would further enhance this clinical effectiveness.

Accurate pre-treatment optimization and real-time adaptations of the administered heating may be crucial steps for further progress and widespread clinical adoption of hyperthermia [5]. Maximization of the heating is nowadays tackled by phased array applicators. Optimization of treatment settings plays a central role in pre-treatment planning especially for challenging anatomical sites such as the head & neck (H&N) region [5] and when real-time feedback control is absent [17, 18]. Hyperthermia treatment planning (HTP) involves obtaining the optimal complex excitation coefficients (phases and amplitudes) of the signals feeding the applicator. The objective of this procedure is to induce a homogeneous temperature over a given target area, while avoiding high temperatures, i.e. "hot-spots", in healthy tissues. Given the relation between the specific absorption rate (SAR) and the temperature distribution [19], treatment quality surrogates based on both have been defined and used to obtain the desired target conformal temperature increase [5, 20]. The problem of shaping the intensity distribution of an electromagnetic field is a canonical and fundamental problem of wave physics, which is relevant in many applications. In this thesis, novel paradigms for the field intensity shaping have been introduced and particularized to deal with the hyperthermia treatment planning.

The remainder of this Chapter is organized as follow: Sect 1.2 reports a brief review of the many different planning routine so far proposed/clinically tested. The general HTP process is given in Sect. 1.3 with specific reference to the planning in H&N, since that was used as clinical bench-test in this thesis.

1.1 How to *optimally* plan an hyperthermia treatment?

Whether the SAR or temperature distribution should be optimized is still a topic of debate amongst hyperthermia researchers [20]. Optimizing the temperature distribution would seem the most natural approach, since increasing temperature is of course the basis for therapeutic effectiveness of a hyperthermia treatment [21]. However, although thermal optimization intuitively relates better to measured temperatures, a systematic study to assess the actual relation between the predicted temperature and the clinical outcomes is to the best of our knowledge not available yet. For SAR, a study by Lee et al. [22] demonstrated that a relation exists between SAR coverage indicators and clinical outcome of the hyperthermia treatments. In addition, temperature based optimization generally exploits global optimizers, which are affected by high computational cost, problem-specific parameters tuning. Also, they are applicable only to limited-size problems, since optimization complexity rises exponentially with the number of unknowns (i.e., number of antennas) [23]. Since computation time is not unlimited and parameter tuning might be different for each clinical scenario, global optimizers may in practice not always deliver the optimal solution. While some efficient approaches have been proposed in the literature [24–26], performances cannot be guaranteed for all possible cases. In this respect, Canters et al. [27] showed that, for the case of deep pelvic hyperthermia, the benefit of directly optimizing the temperature pattern is lost under the very large uncertainties of thermal modeling. Moreover, note that the more accurate thermal dependent model [28] strongly impacts on the overall computational burden. Conversely, SAR is directly related to the complex excitation coefficients via the Maxwell equations. Hence, SAR is usually correctly predicted by a planning system which is not the case for the temperature distribution because of the assumptions in thermal modeling. Further, SAR can be experimentally validated within a quality assurance procedure. Hence, SAR performance of a hyperthermia system can be computationally and metrologically controlled [5]. Whatever the case, while results in contrast with the one in [29] were found by de Greef et al. [30, 31], optimizing the SAR pattern is, anyway, faster than temperature optimization, since it does not imply solving the bio-heat equation as well.

On the basis of the attractive features recalled above, many SAR based optimization approaches have been proposed in the literature. Some approaches aim at maximizing the SAR within the target volume while minimizing it in the surrounding healthy tissues. Global optimizers have been usually invoked to address this problem as in [32, 33]. With the same spirit, the group of prof. Hagness proposed a technique based on time multiplexing of multiple beam-formers in the context of brain

hyperthermia treatment [34]. Hereto, while a clinical assessment is lacking in the literature, the optimization problem was conveniently cast as a eigenvalue problem. In [35,36], HTP optimization routine based on the well-known time-reversal (TR) approach [37] are proposed. While very intuitive, straightforward and with a negligible computational time, such approaches suffer from two main drawback: 1) the need of the so-called time reversal mirror (i.e., a spherical applicator surrounding the region under test), difficult in many cases, and 2) the impossibility of controlling hot-spot arising. Among the others, a relatively recently proposed approach is the so-called focusing via constrained power optimization (FOCO). In the first place, such an approach was proposed in the antenna framework for the optimal synthesis of pencil beams [2]. The similar mathematical formulation of such a problem with the one at hand led to its feasibility in HTP [19]. FOCO allows to focus the SAR distribution in the target volume and at the same time enforce hot-spot-limiting constraints in the healthy tissues. Being cast as a convex programming problem, FOCO does not require global search algorithms and it delivers the globally optimal solution regardless of problem size (i.e., number of unknowns/antennas) or parameters tuning [19]. On the other side, as compared to TR-based approach, the computational time is expected to be higher. Lastly, FOCO was shown to be relatively insensitive to uncertainties on both thermal and electromagnetic [19]. However, the performance of FOCO in a clinical setup is unknown.

1.2 The Hyperthermia Treatment Planning Work-Flow

Planning an hyperthermia treatment can be identified as a 6-steps procedure as shown in Fig. 1.1. In the following we describe the clinical HTP workflow as implemented at the Erasmus MC [20, 33]. While software or technical/technological implementation could vary between institutions, the spirit as well as the outcome is to be considered equivalent. In this thesis we specifically dealt with the very challenging clinical scenario of patients with H&N cancer. As such, in the following, specific hints to this case are given.

The first two steps aim at building up a 3-D patient specific model. This is created by delineating the various tissues starting from computerized tomography scans and making use of a custom atlas based auto segmentation routine followed by a manual adjustment [38]. The segmented tissues of the generated 3-D patient-specific models are then associated to group optimized constant electromagnetic and thermal tissues parameters accordingly to [33,38,39]. Then, 3-D patient-specific models are imported

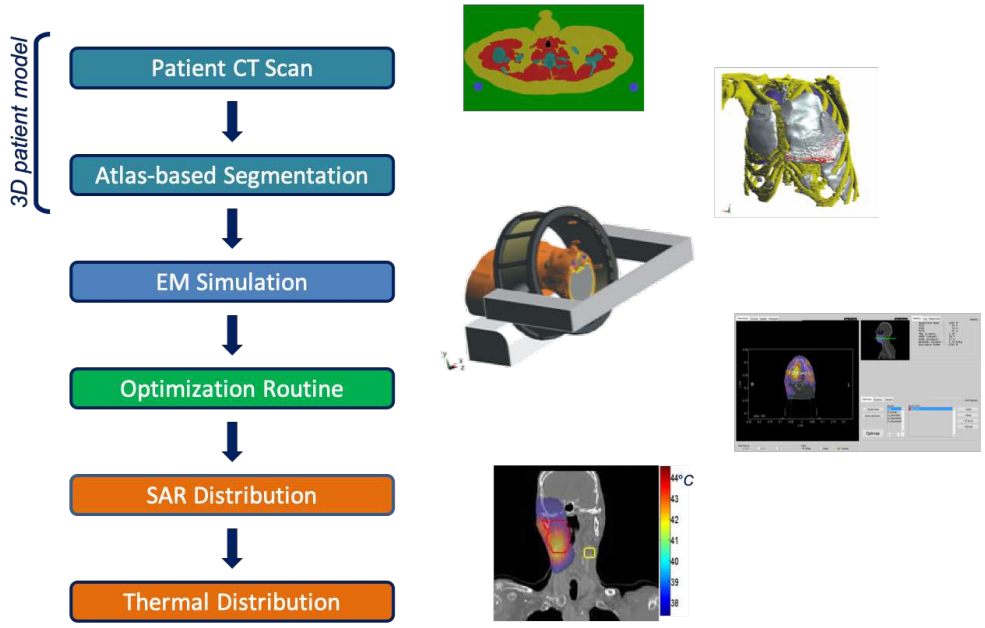

Fig. 1.1. Schematic description of the HTP workflow

into a full wave numerical simulator and simulated together with the designed applicator.

Many different phased array applicators have been developed and proposed so far both for the deep pelvic and the H&N. Applicators vary in the number of antenna as well as in antenna element in itself. Usually a water bolus fills the space between the applicator and the patient to avoid undesired heating that may arise at the patient's skin and to enhance electromagnetic coupling [40]. Examples are the RHOCS system (18 antennas), the BSD-2000 Sigma-Eye (12 antennas), the AMCs systems (4/8 antennas) [41], the H&N applicators from Trefná et al. (10/16 antennas) [42,43], the hybrid MRI system (8/16 antennas) from the group of Winter et al. [44, 45]. For the H&N, the HYPERcollar3D is nowadays the only clinically tested applicator world-wide.

The third step of HTP consists in design the applicator and to simulate it together with the generated 3-D patient model. Using this setup, the total field is computed for each antenna. The total electric field generated by each antenna are then used as elementary brick to be combined to generate the desired patient-specific heating pattern. Hence, the fourth step of HTP consists in optimizing the SAR or the temperature to determine the complex (phase and amplitude) excitation coefficients feeding the applicator. At the Erasmus MC, a in-house optimization routine has been implemented and is nowadays clinically adopted for both deep pelvic and H&N hyperthermia. This

optimization approach has been reported in the following paragraph since, in this thesis, it has been used as a comparison benchmark.

Finally, the last two steps of HTP concern the evaluation of the treatment both in terms of SAR and temperature by means of quality metrics which are known to be correlated to good outcome of a treatment. These clinically adopted standard HTP quality metrics [29] are reported and discussed in Appendix A.

1.2.1 Treatment Planning Approach: A Clinically Tested Example

A possible strategy, which is the implemented in clinical Visualization Tool for Electromagnetic Dosimetry and Optimisation (VEDO) is the so-called Target to Hot-Spot Quotient PSO-optimized [33]. Such an approach is nowadays used in the clinic for different applicators in both deep pelvic and H&N patients. In this paragraph some details are given concerning this optimization approach since it was used as a comparison benchmark in the following analysis.

This approach is based on the notion that planning in hyperthermia treatment is a multi-objective optimization problem with a twofold aim: **1)** maximizing the SAR within the target volume and **2)** minimizing the SAR in hot-spots in healthy tissues. Starting from this consideration, the cost function is the Target to Hotspot SAR Quotient. This latter is defined as:

$$THQ = \frac{< SAR_{target} >}{< SAR_{HS} >} \tag{1.1}$$

where $< SAR_{target} >$ is the mean SAR in the target volume and $< SAR_{HS} >$ is the average SAR in hotspots, defined as the 1% volume of healthy tissue volume where the highest SAR occurs [33]. Note, being the ratio of the average SAR in two different volumes, THQ is a-dimensional.

This optimization problem is non-convex and it is tackled by a global optimizer. Hereto, the well-known particle swarm optimization (PSO) was used exploiting ad-hoc customized settings [33, 46].

1.3 Structure and Relevance of the Thesis

While the debate on whether SAR-based or temperature-based optimizers have to be considered still open, this thesis work is focused on SAR-based optimizers because of its many attractive features as from Sect. 1.2. Amongst the many approaches proposed in the literature, a relatively recently proposed approach is FOCO. An interesting remark about FOCO is that it was firstly introduced by Isernia et al. [2] within the

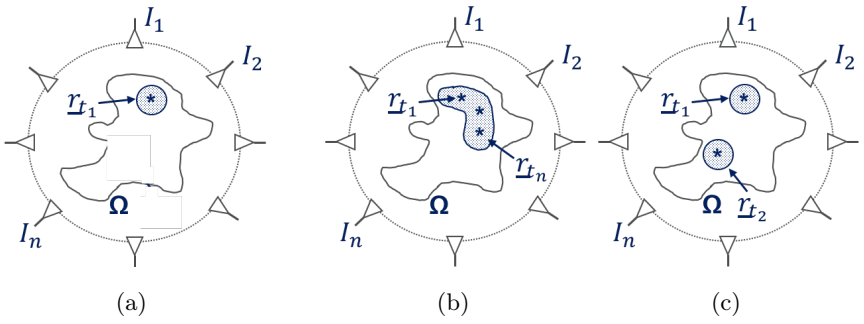

Fig. 1.2. Schematic view of the phased array applicator surrounding the domain of interest (Ω) and of the target volume (HTV) in case a focused (a) or uniformly shaped (b) or multi-spot focused (c) SAR distribution is desired.

framework of antenna synthesis problems. Because of its very general formulation, FOCO is able to deal both with ultrasound and electromagnetic wave as well as to be exploited within HTP. FOCO, indeed, aims at focusing the power deposition within the HTV while constraining it to prescribed levels in the healthy tissues, i.e., limiting hot-spots. A relevant feature of FOCO is that it is formulated in terms of a CP problem, hence it is operator-independent as it ensures the global optimality of the solution regardless of the problem size/complexity. Here, for the first time FOCO has been translated into the clinical work-flow and tested in 3-D patient models. In this thesis, a clinical assessment have been pursued within the very challenging clinical scenario of patients with H&N cancer. This scenario presents a very good case for assessment of the benefit of novel HTP optimization routines. In fact, target conformal heating is possible and therefore HTP is pivotal and routinely used [5] and temperature simulations have been extensively validated and a dedicated set of tissue properties are available [39]. Therefore, this scenario is highly suited for our aims in terms of predicted treatment quality (SAR and temperature) and computational costs. For benchmarking, we used the clinic adopted optimization routine, as presented in [11] and reported in the previous Section.

Our clinical results suggested that the present optimization routines were not always able to successfully deal with the locally advanced tumors (i.e., the larger target volumes). In other words, "just" focusing the SAR distribution in a target point set into the HTV, schematically reported in Fig. 1.2.(a), was shown to be a sub-optimal solution for such challenging cases where a uniformly shaped SAR distribution is needed. Hence, the novel paradigm of SAR shaping, as opposed to SAR focusing, is herein proposed and tested. Hence, the work carried out is separated into two Chapters: one including the optimization strategies aimed at focusing the SAR distribution and one

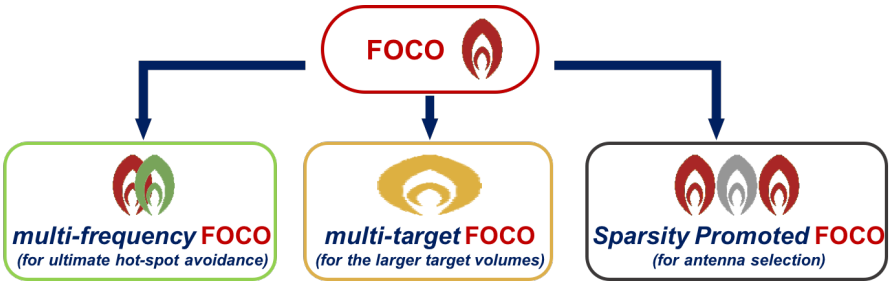

Fig. 1.3. Graphical view of FOCO and its derivations.

including the optimization approaches aimed at shaping the SAR distribution over an extend HTV possibly with irregular contours. Note, the shaping paradigm is not only related to the generation of a uniformly shaped distribution but also of a multi-spot focussed one as schematically shown in Fig. 1.2.(c). This could be of great interest to large tumors at challenging locations with sensitive tissues, such as glioblastoma multi-forme [47, 48].

The proposed approaches are divided into the ones aimed at a focusing and the one aimed at shaping the power deposition distribution, in Chapter II and in Chapters III-IV respectively. In Chapter II, named *Constrained Power Focusing*, the general mathematical formulation of FOCO has been modified in order to address different clinical needs. Versatility, amongst all, is the more remarkable feature of FOCO. Following, Chapter III, named *Un-Constrained Power Shaping* contains an un-constrained SAR shaping approach developed exploiting both the theoretical finding of this thesis and the well-known TR method. However, besides the many remarkable perks of TR, its intrinsic inability in controlling undesired heating triggered the development of the only constrained shaping approach based on a convex-programming problem in the literature, proposed in Chapter IV, named *Constrained Power Shaping*.

Three considerations are in order. Firstly, this thesis represent the creation of a pool of different focusing/shaping strategies inspired by different clinical needs, at the same time with a general methodological point of view leading to their possible application in different fields. Second achievement of this thesis is that for the first time in the Hyperthermia Community the problem of shaping, as opposed to focusing, the power deposition has been recognized and properly tackled. Thirdly, a remarkable novelty of this thesis is the introduction of constrained convex-programming-based optimization strategies into the hyperthermia treatment planning framework. Lastly, this thesis represents a solid merge between theory and application since the developed methodologies were tested on actual patient data thanks to the collaboration with the Erasmus MC.

Besides the unconstrained shaping approach proposed in Chapter III, Figure 1.3 aims at giving a pictorial view of FOCO and its derivation proposed in this thesis. Specifically, these are:

- **multi-frequency FOCO** (mf-FOCO), in Chapter I, is based on the idea that hot-spot spatial collocations could change with frequency. Hence, exploiting such a feature, adopting multi-frequency applicators one could (in principle) avoid hot-spots occurrence (or lower their impact) [7].
- **sparsity promoted FOCO** (sp-FOCO), in Chapter I, was (recently) introduced to address the need of "optimally" selecting the active elements of a given applicator in a patient-specific fashion [49].
- **multi-target FOCO** (mt-FOCO), in Chapter IV, aims at uniformly shaping the SAR over an extended possibly with irregular contours target area (i.e., late stage tumors). Nowadays this task is not efficiently addressed by the clinically adopted algorithms [11].

2

Constrained Power Focusing

In this Chapter three different optimization approaches addressing different clinical needs are introduced and developed. The three constrained approaches aim at focusing a wave-field in a target point and based on FOCO. In Sect. 2.1, the general formulation of FOCO is reported together with a comparative clinical assessment against the optimization approach adopted at the Erasmus MC. Following, in Sect. 2.2, the problem of optimally selecting a subset of antennas from an oversized applicator (where more antennas than amplifiers are available) is tackled by merging FOCO with concepts taken from the compressive sensing theory. Again, a comparative assessment against the clinically procedure adopted at the Erasmus MC is provided. Finally, in Sect. 2.3, aimed at further decreasing undesired heating in healthy tissues, the extension of FOCO to the case of multi-frequency electromagnetic field is reported together with a proof of concept on 2D realistic phantoms. The mathematical formulation of the proposed approaches (both in this Chapter and in the following) are reported under a common mathematical framework which is briefly given in the following.

With reference to the scheme reported in Fig. 1.2.(a), and indicating $\underline{r} \in \Omega$ a generic point of the 3D region of interest (Ω), the SAR can be expressed as:

$$SAR(\underline{r}) = \frac{\sigma(\underline{r})}{2\rho(\underline{r})}\left|\mathbf{E}(\underline{r})\right|^2 \tag{2.1}$$

Where σ is the conductivity $[S/m]$, ρ is the mass density $[kg/m^3]$ and $\left|\mathbf{E}(\underline{r})\right|^2$ is the squared amplitude of the total electric field generated by the "weighted" N monochromatic sources surrounding Ω.

Assuming $\mathbf{\Phi}_n = \Phi_{x,n}\mathbf{i}_x + \Phi_{y,n}\mathbf{i}_y + \Phi_{z,n}\mathbf{i}_z$ the total electric field induced by the unitary excited n-th antenna in Ω when all the other antennas are off, the overall electric field, i.e., $\mathbf{E} = E_x\mathbf{i}_x + E_y\mathbf{i}_y + E_z\mathbf{i}_z$, in a generic point in the domain of interest can be expressed as:

$$\mathbf{E}(\underline{r}) = \sum_{n=1}^{N} I_n \mathbf{\Phi}_n(\underline{r}) \tag{2.2}$$

where $I_n (n = 1, 2, ..., N)$ represent the complex excitation coefficients of the signals feeding the different applicators.

2.1 Focusing via Constrained Power Optimization

FOCO aims at focusing the power deposition onto a target location "properly" set within the target volume, while constraining it to predisposed levels in the healthy tissues to prevent treatment limiting hot spots. From the physical point of view, FOCO pursues the focusing of the electromagnetic field pattern. Note the choice of the target point is in some sense a "degree of freedom" of the procedure.

Considering a target point properly set within the target area, say $\underline{r}_t \in \Omega$, a generic constrained focusing problem could be stated as:

Determine the set of the array's complex excitations coefficients such to maximize the squared amplitude of the field in the target point, i.e., $\left|\mathbf{E}(\underline{r}_t)\right|^2$*, while enforcing arbitrary upper bounds in the rest of the domain of interest.*

This maximization problem is non-linear and belongs to the class of NP-hard problems [23], since the considered cost functional $\left|\mathbf{E}(\underline{r}_t)\right|^2$ is a non-negative quadratic polynomial with respect to the unknowns I_n. As such, by using local optimization procedures the global optimality of the solution is not ensured.

On the other hand, when one of the field components, $(E_i(\underline{r}))$, can be considered to be dominant above the other ones, FOCO circumvents the above difficulty by exploiting the degree of freedom on the field phase reference, assuming that the field in the target point is real [2, 19].

Under such a circumstance, the problem can then be stated as:

Find I_n $(n = 1, ..., N)$ *such to:*

$$max\{\Re\{E_i(\underline{r}_t)\}\} \tag{2.3}$$

subject to:

$$\Im\{E_i(\underline{r}_t)\} = 0 \tag{2.4a}$$

$$\left|\mathbf{E}(\underline{r})\right|^2 \leq \mathcal{MF}(\underline{r}) \qquad \underline{r} \in \Omega \setminus \Pi(\underline{r}_t) \tag{2.4b}$$

where $\Re\{\cdot\}$, $\Im\{\cdot\}$ and $\Pi(\underline{r}_t)$ represent the real part, the imaginary part and the target volume, respectively.

As constraints (2.4a)-(2.4b) define a convex set in the space of the unknown unknowns [2], and considering that cost function (2.3) is a linear function of the unknowns, the overall constrained focusing problem can be now conveniently cast as a

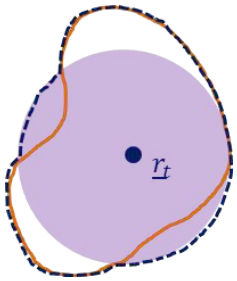

Fig. 2.1. Sketch of the mask function adopted for FOCO. CTV is in plain orange line, RS in light purple, Π_{FOCO} in dotted blue and the target point as the blue dot.

convex programming problem. As such, the globally optimal solution can be efficiently determined via local optimization procedures.

Note constraint (2.4b) allows to enforce an upper bound on the power deposition outside the chosen target volume, $\Pi(\underline{r}_t) \in \Omega$, by means of a non-negative function $\mathcal{MF}(\underline{r})$ (a *"mask"* function). The "mask" function is a non-negative arbitrary function that allows enforcing patient-specific constraints on the power deposition outside the chosen target area. Higher weights can be applied to tissues exhibiting higher power losses to counteract undesired heating.

The target volume Π_{FOCO} is defined as a non-isotropic volume expansion of the so-called Hyperthermia Target Volume (HTV) which, following Radiotherapy, generally corresponds to the Clinical Target Volume (CTV) [50]. Figure 2.1 schematically shows how Π_{FOCO} was defined. Starting from the CTV delineation, the margins used by Π_{FOCO} include the volume of a minimum focusing sphere, which we define as a "resolution sphere" (RS). Considering the physical limitation of the focusing capability of any phased array applicator in tissue, as theoretically and experimentally shown in [51, 52], this RS is a sphere with a diameter of $\approx \lambda_m/3$, being λ_m the wavelength in a medium with average dielectric tissue properties. The RS is centered at the HTV centre of mass, i.e. the "target point" ($\underline{r}_t$). Note that Π_{FOCO} is used only in the optimization phase. All distribution evaluations have been done using the HTV for a fair comparison.

2.1.1 Clinical Assessment

In the following we benchmarked FOCO to the clinical adopted procedure, i.e., THQ PSO-optimized, detailed reported in Sect. 1.3.1. The considered dataset consists of twelve 3D patient models generated during HTP for patients with H&N cancer that were planned for treatment with the HYPERcollar3D and as from Sect. 1.3. The comparison was carried out exploiting both SAR-based and temperature-based qual-

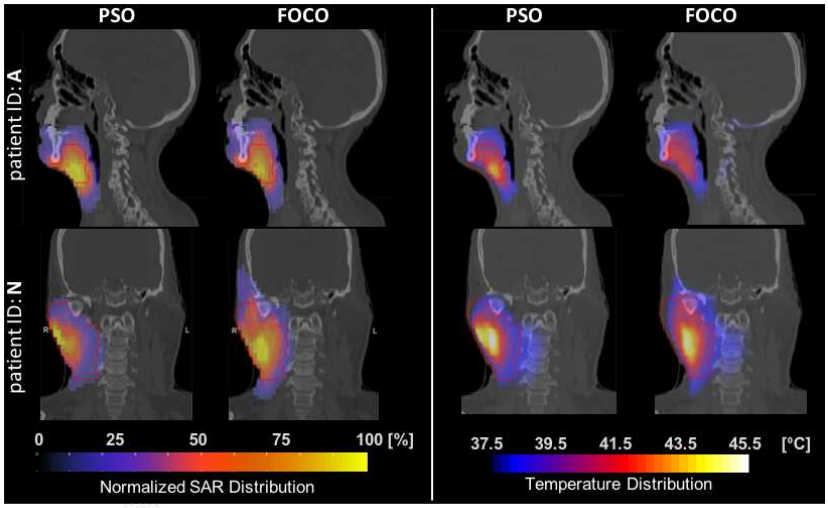

Fig. 2.2. Temperature and normalized SAR distribution related to case A on a sagittal view, and N on a coronal view obtained by means of THQ PSO optimized and FOCO.

ity metrics as reported in Appendix A. In the following the subscripts PSO and FOCO have been added to indicate the metrics respectively related to the clinical benchmark and FOCO. In this study, the planning results are ultimately evaluated using the temperature distribution, which is simulated using the Penne's Bio-Heat Transfer Equation [53]. The temperature distribution was achieved by adjusting SAR to a maximum of 44°C in normal tissue, i.e. outside the HTV. Lastly, since optimization time is relevant in a real-time re-optimization scenario, in this extensive clinical assessment also the computational time has been monitored and indicated as t_{FOCO} and t_{PSO}. All simulations are run on a pc equipped with an Intel Core i7-3770 (3.4GHz) CPU and 8GB of RAM.

In total, twelve patient models were included, of which one was planned for treatment, but not treated due to insufficient TC25 (see Appendix A), and two patients were treated using a reduced HTV. These cases where specifically included to investigate if FOCO would not only improve the optimization of currently treated patients but also enable to expand the number of treated patients.

Results

As an initial verification step, the Dice similarity coefficient[1] [54] between Π_{FOCO} and HTV was evaluated, obtaining a value of, i.e., ≈ 1, which demonstrates their excellent overlap.

Table 2 and Table 3 report TC25, THQ, T50 and computational time, as well as patient details including target volume size. The target volumes ranged from 19.1 to $287.1cm^3$. As expected, THQ for FOCO is on average $\approx 20\%$ lower than THQ_{PSO} coherently with the circumstance that THQ is the optimization parameter in the clinical PSO-based strategy. Conversely, on average, target coverage and T50 were found to be approximately equal, with a slight improvement with FOCO, since $TC25_{FOCO}$ was 3% greater and ΔT50 increased by 0.05°C. Moreover, the computational time required by FOCO was $0.36 \pm 0.14min$, which is 44% lower than $(0.61 \pm 0.53min)$.

Figure 4.3 depicts the normalized SAR distribution and the inherent temperature distribution obtained by means of FOCO and THQ PSO optimized for patient IDs A and N. This figure shows that the optimization results for FOCO and THQ PSO are indeed very similar in small tumors, but differ greatly in large tumors. Specifically, FOCO provides a much higher SAR coverage in large target volumes, while reducing SAR in normal tissue. Table 2 shows that FOCO indeed performs much better for these patients, i.e. $\Delta TC25 = +5\%$ and $\Delta T50 = +0.39$°C on average for patients A-C, N and M. Note that the target volumes of this group are all larger then >40 cm^3, with an average volume size of $145.4 \pm 111.6cm^3$.

Fig. 2.3 depicts the SAR and temperature comparison parameters for PSO and FOCO. PSO was better in terms of THQ and the metrics were equal in terms of TC25. In this figure, green circles have been added to mark the large TV cases.

Discussion

This analysis demonstrates the clinical capabilities of FOCO, a recently proposed method for hyperthermia treatment planning, based on constrained SAR optimization via convex programming. The assessment has been carried out in an actual clinical scenario and the outcomes compared to the clinically used benchmark, i.e., THQ PSO optimized planning [11]. The results, showed that, although FOCO overall performs comparably to the benchmark, there is a tendency to outperform this benchmark for target volumes above $\approx 40cm^3$ in terms of T50. In ≈50% of the analyzed cases (i.e.,

[1] The Dice coefficient is a statistic used for comparing the similarity of two samples and is equal to twice the number of elements common to two sets divided by the sum of the number of elements in each set [54].

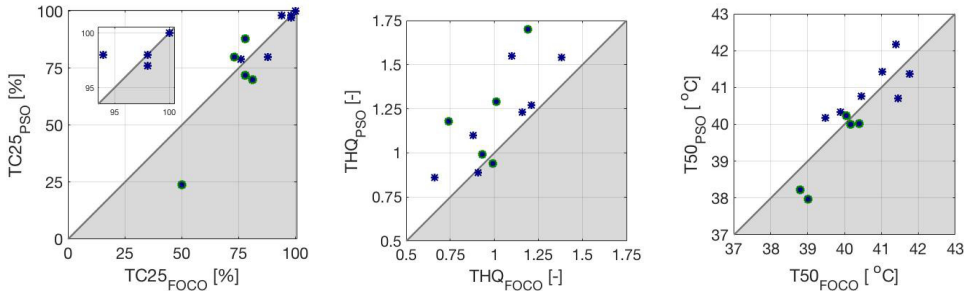

(a) (b) (c)

Fig. 2.3. SAR and temperature distribution performances comparison on TC25 (a) and THQ (b) and T50 (c). Note that the group of large targets contains untreated cases to analyze if FOCO would enable treating these patients. Large target volumes have been marked with additional green circles. Note, in (a) two cases are overlapped - see Table 1.

patient D to L) a negligible average difference was found on TC25, corresponding to a ΔT50 of 0.05°C and to an average TV of $30 \pm 9 cm^3$. In the remaining cases, related to a bigger average TVs of approximately $145.4 \pm 111.6 cm^3$, a ΔTC25 equal to +5% and a ΔT50 equal to +0.39°C was found. This analysis suggests that similar performance can be achieved by the two planning approaches for the average target volume in all locally-advanced diseases, whereas FOCO delivers a higher average for the larger target volumes in this group compared to the THQ PSO optimized solution. On the other side, the discordant results found for patient D and M indicate that further investigations are needed to better evaluate the large target volume threshold.

In alignment with the study of Wust et al. [55], we found that performance of THQ based optimization is worse for larger and more complex HTVs. Notably, a crucial aspect of SAR optimization is the proper choice of the cost function, as the problem is multi-objective. In the case defocusing is needed, as required for a relatively small wavelength relative to the target region area, optimizing the THQ yields sub-optimal solutions, see Fig. 2. Interestingly, the possibility of achieving a tighter control on the spatial distribution of SAR, by properly positioning the target point exploited by the FOCO procedure, would allow to overcome such a limitation.

In the current study, we used SAR optimization and exploited temperature simulations for relative assessment of optimization performance. The reason for this approach is that current temperature simulations are prone to severe uncertainties due to uncertainties in tissue cooling parameters, which can vary in time, within tissues, between tissues and between patients. The impact of tissue cooling uncertainties for H&N hyperthermia are unknown. For deep pelvic hyperthermia, Canters et al. [29] have shown that large uncertainties of thermal properties denies the benefit of opti-

Patient ID	Tumor Location	TV [cm^3]	TC25 [%]		THQ [-]		T50 [^oC]	
			PSO	FOCO	PSO	FOCO	PSO	FOCO
A	NNM	54.1	80	73	1.29	1.01	40.01	40.18
B*	Oropharynx	239.4	72	78	0.94	0.99	40.01	40.41
C**	Larynx	40.1	70	81	1.70	1.19	37.97	39.01
D	NNM	34.3	80	88	1.55	1.10	40.33	39.88
E	PG	36.6	98	98	0.89	0.91	40.71	41.46
F	Oropharynx	34.5	79	76	0.86	0.66	40.17	39.48
G	Oropharynx	28.0	100	100	1.27	1.21	40.77	40.47
H	Hypopharynx	43.4	97	98	1.54	1.38	41.43	41.03
I	Oropharynx	19.1	100	100	1.23	1.16	41.38	41.77
L	Oropharynx	21.8	98	94	1.10	0.88	42.17	41.39
M	Oropharynx	106.5	88	78	0.99	0.93	40.24	40.04
N**	NNM	287.1	24	50	1.18	0.74	38.23	38.79
	mean	78.7±89.7	82±21	85±15	1.21±0.28	1.01±0.21	40.28±1.21	40.33±0.96
	$mean_{(TV>40cm^3)}$	145.4±111.6	67±25	72±12	1.22±0.30	0.97±0.16	39.29±1.10	39.64±0.73

Table 2.1. Patient and treatment characteristics, i.e. tumor volume, location, TC25, THQ and T50 for the analyzed HTP approaches. The patient indicated with $*$ was planned for treatment with the HYPERcollar3D, but not treated due to insufficient TC25. Patients indicated with $**$ were treated using a reduced HTV, which was smaller than the radiotherapy treatment volume. NNM and PG stand respectively for Neck Node Metastasis and Parotid Gland.

mizing the temperature distribution. Also, Drizdal at al. [56] found large differences between predicted target coverage for different thermal tissue property models, but a strong correlation between the coverage derived from SAR and H&N specific constant tissue cooling base temperature predictions, as also used in the current study. These results shed a different light on the ongoing debate on SAR or temperature optimization. They also stress the crucial importance of more research on the validation of thermal modelling and on the assessment of dynamic, temperature dependent, tissue cooling properties. In future, with increasing knowledge on temperature dependent and transient tissue cooling properties, temperature optimization is generally expected to start replacing SAR optimization. However, given the large uncertainties in the currently available tissue properties at present, temperature predictions are primarily useful for comparative dosimetry, as also indicated by [57].

In the comparison, the common inability to define optimal treatment outcome was faced. In the clinic, thermal dose effect relations advocate the use of CEM43°CT90 [58]

Patient ID	t [min]	
	PSO	FOCO
A	0.40	0.28
B*	0.49	0.41
C**	0.65	0.26
D	0.30	0.40
E	0.50	0.24
F	0.42	0.33
G	0.52	0.33
H	0.43	0.25
I	0.51	0.41
L	0.49	0.38
M	2.28	0.32
N**	0.39	0.77
mean	0.61±0.53	0.36±0.14

Table 2.2. Computational times related to the analysis reported in Table 2.3.

and/or T50 [59]. In contrast to measurements, which are often from a limited number of locations, thermal modelling holds the advantage that techniques can be compared using the full 3D distribution. Unfortunately, thermal modelling is prone to severe thermal tissue property inaccuracies and hence temperature simulation accuracy is limited [60]. Current thermal modelling ignores the considerable impact of the temperature dependence of the tissue properties [39], which can seriously hamper technology comparisons [56]. In this work, we analyzed both temperature (T50) and SAR (THQ, TC25) quantifiers. Power was increased in the temperature simulations until the maximum temperature in normal tissue reached 44°C, to match the clinical procedure in patients are treated up to feedback by complaints. As such, we focussed our attention to relative differences rather than absolute values. Note that, for the particular case of H&N hyperthermia, Verhaart et al. [39] showed that T50 can be predicted with a median accuracy of 0.8°C, even when ignoring thermoregulation. Hence, our simulations are expected to be sufficiently predictive since the tissue cooling values have been specifically optimized for the H&N. By exploiting both SAR and temperature indicators, we assume that our analysis provides the optimal combination of relative metrics to compare optimization performance from a clinical point of view.

While FOCO delivers the globally optimal solution of its optimization functional, in practice THQ_{FOCO} values were lower than THQ_{PSO}. Of course, THQ represents the cost function in PSO in the current clinical procedure, whereas FOCO incorpo-

rates a different cost function. Hence, THQ would be a biased quantifier for comparisons between THQ PSO and FOCO. Moreover, looking at the relation between THQ and T50 in H&N hyperthermia, it is questionable whether higher THQ values are necessarily related to a higher performance in terms of T50. Hence, while THQ unquestionably is a relevant optimization function and predictive for T50 (in deep pelvic hyperthermia [29]), our investigation suggests that a work similar to the one in [29] needs to be carried out for the case at hand. Additionally, the conflicting results between the SAR and temperature metrics related to case A, depicted in Fig. 4.3, suggested a possible hybrid FOCO optimization procedure that exploit the fast SAR optimization with a mask function created on the basis of the temperature field hot-spots. Concerning the results of case A, it is possible to state that while FOCO is outperformed on TC25, this does not hold true on the temperature quantifier, T50.

From a computational point of view, FOCO is approximately 44% faster than THQ PSO. Since FOCO is cast as a convex programming problem, it does not exploit global optimizers that may suffer from larger computational times. In addition, global iterative optimizers may also suffer from sub-optimal solutions which, depending on the optimization space, could lead to a lower reproducibility. On the other side, FOCO is able to reduce computational time and ensure a less operator-dependent solution. From a clinical prospective, the improvement of the computational time goes towards the real-time adaptation of the administered heating, e.g., in case of patients complains. Moreover, in such a case an additional constraint on the sensitive area would be enforced. Assuming that the new constraints would not deliver an optimization result far from the previous one, FOCO can take profit from such a circumstance (using the first optimization solution as an improved initial guess) and further reduce the computational time. The same approach is impossible using global optimizer.

Moreover, accordingly to the clinic practice, in the present work a voxel size equal to $5 \times 5 \times 5mm$ has been adopted to keep the computational time of THQ-PSO optimized curbed. On the other side, FOCO would allow to increase the resolution (i.e., using a smaller voxel size) as well as an higher number of antennas at a limited increase of the computational time. Such a feature is of particular interest in magnetic resonance compatible applicators with PCB[2] type antennas [61]. In this case higher requirement in terms of resolution for the treatment planning are needed [62]. Here also the inevitable impact of electromagnetic and thermal uncertainty of tissue parameters on both FOCO and THQ PSO must be taken into account, to better understand the combined impact. Finally, note that GPU[3] implementation is feasible

[2] Printed Circuit Board

[3] Graphic Processor Unit

also for FOCO, and future plans are aimed at comparing optimization time improvement against THQ PSO.

Another improvement in FOCO could be the extension to all three components of the field. FOCO, indeed, is assuming that the axial component of the electric field was dominant above the others. Hence, even though the amplitude of the z-component was on average 3 ± 0.8 times greater than the x- and the y-component in the FOCO target point, FOCO performance versus PSO optimization could be improved when applied on three components of the field. This could, for example, affect the analysis of patients A and N, where the polarization may play a relevant role. Hence, we can conclude that further improvements could be achieved by exploiting the full vector nature of the field, determining the field intensity polarization in the target point leading to an improved power deposition distribution [63].

2.2 Sparsity Promoted FOCO for Antenna Selection

Accurate pre-treatment optimization and real-time adaptations of the administered heating includes the optimally design of both the applicator and the complex excitations (phases and amplitudes) feeding its elements [5].

Parallel to an optimal planning strategy (either SAR- or temperature-based), the second key ingredient of hyperthermia is the proper design of the phased antenna array applicator. Hereto, constructive interference of fields radiated by each antenna is exploited to maximize the SAR in the target area while avoiding over-heating of the healthy tissues, i.e., hot-spots. This task involves different design parameters. By increasing the frequency, for instance, a more target conformal heating pattern can be achieved, although a price is paied in terms of a reduction of the penetration depth (thus lower SAR levels). For a fixed frequency, the heating pattern can be optimized by both increasing the number of transmitting elements (coherently with [64]) and/or optimizing the array geometry [65].

The need of treating tumors positioned in different anatomical regions triggered researchers to propose different applicators with various geometries, (larger) antenna element number and working frequency, e.g., the RHOCS system (18 antennas), the BSD-2000 Sigma-Eye (12 antennas), the AMCs systems (4/8 antennas) [41], the head and necks applicators from Trefná et al. (10/16 antennas) [42, 43], the hybrid MRI system (8/16 antennas) from the group of Winter et al. [44, 45] and the HYPERcollar3D (20 antennas) [40]. As a general concern, given the necessary patient-specific aspect of the problem, increasing the number of radiating elements may represent a straightforward strategy to improve SAR levels into arbitrary positioned hyperthermia target volume (HTV), as it would enable a larger number of degrees of freedom readily available for the optimization. However, each radiating element requires a power amplifier which, because of the required specifics, has a non-negligible impact on the overall system cost [40]. As a result, taking into account that only a limited number of amplifiers are usually available, and that each treatment is strongly case-specific, the development of an antenna selection procedure is advisable.

The problem we are dealing with is that of minimizing/reducing the arrays active elements number able to maximize the SAR within the target volume and, at the same time, avoid undesired heating in heathy tissues. Hence, the sparsity of the solution, i.e., the complex excitation coefficients, has to be promoted. Hence, many concepts can be profitably borrowed from the CS theory [49, 49, 66, 67].

In the following, we present and test the feasibility of a novel optimization tool that is able to optimally select a desired number of active antennas from a given applicator

able to maximize the SAR deposition in the HTV while avoiding hot-spot occurrence. The proposed sparsity promoted FOCO (SP-FOCO) determines the optimal active elements configuration (and the corresponding excitations) exploiting possible constructive and/or destructive interference of the fields generated by each element of a given applicator. The development of the proposed approach takes advantage both from FOCO and from the CS theory [49].

2.2.1 The proposed approach

The proposed approach is based on FOCO. Hereto, enforcing that just a certain number of antennas (L) from the whole set (N_{wa}) has an excitation different from zero could be formulated as:

Find I_n $(n = 1, ..., N)$ *such to:*

$$max\{\left|\mathbf{E}(\underline{r}_t)\right|^2\} \tag{2.5}$$

subject to:

$$\left|\mathbf{E}(\underline{r})\right|^2 \leq \mathcal{MF}(\underline{r}) \qquad \underline{r} \in \Omega \setminus \Pi(\underline{r}_t) \tag{2.6a}$$

$$\|I_n\|_{l_0} \leq L \tag{2.6b}$$

where $\|\cdot\|_{l_0}$ is the pseudo l_0 norm (counting the number of elements different from zero in the sequence) [66].

Unfortunately, the optimization problem (2.5-2.6a,b) would be a very hard one (belonging to the NP-class hard class [23]). Analogously to FOCO, a first simplification can be gained when one of the field components ($E_i(\underline{r})$) can be considered to be dominant above the other ones. Then, it is possible to borrow from the CS theory [49,66,67] the circumstance that in optimization (or reconstruction) problems the l_0 pseudo-norm can be often and conveniently relaxed into the l_1-norm. Interestingly, provided a number of hypothesis are fulfilled [49, 66], such a relaxation is "free of charge", in the sense that the global optimum of the original problem holds true.

Hence, by exploiting the above relaxation of the cost function and of the constraints, formulation (2.5-2.6a,b) can be conveniently written as:

Find I_n $(n = 1, ..., N)$ *such to:*

$$max\{\Re\{E_i(\underline{r}_t)\}\} \tag{2.7}$$

subject to:

$$\Im\{E_i(\underline{r}_t)\} = 0 \tag{2.8a}$$

$$\left|\mathbf{E}(\underline{r})\right|^2 \leq \mathcal{MF}(\underline{r}) \qquad \underline{r} \in \Omega \setminus \Pi(\underline{r}_t) \tag{2.8b}$$

$$\|I_n\|_{l_1} \leq \epsilon \tag{2.8c}$$

where ϵ is a tunable parameter.

Constraints (2.8a)-(2.8c) define a convex set in the space of the unknowns [2]. The cost function (2.7) is a linear function of the unknowns. Hence, formulation (2.7, 2.8a,c) is now again conveniently cast as a CP problem. As such, the globally optimal solution can be efficiently determined via local optimization procedures. An alternative formulation to SP-FOCO would aim at determining the minimum number of active antenna elements (and the corresponding I_n) able to deliver a certain a-priori known optimal SAR distribution.

The proper tuning of the sparsity parameter ϵ has a pivotal role in the optimization process [67–69]. In our specific application, we aim at selecting N_A antennas out of the N_{wa} elements of the whole array. As such, large values of ϵ will determine a large number of complex excitation coefficients different from zero, i.e., a number of antennas possibly larger than required. In a dual fashion, small values of ϵ would imply not taking advantage from all the available amplifiers. A possible choice is to set ϵ equal to a fraction of ϵ_{wa} defined as the average $\|I_n^{wa}\|_{l_1}$, where I_n^{wa} are the complex excitations coefficients obtained when optimizing the whole applicator [67]. Hereto, an intuitive choice could be to set ϵ equal to $N_A/N_{wa}\epsilon_{wa}$.

A common practical drawback of sparsity-promotion-based approaches, regardless of the procedure adopted to properly set the ϵ, is that they aim at setting to zero a certain amount of complex excitation coefficients, but, the actual number is not ensured. Therefore, in order to tackle such a limitation, a two step procedure has been devised and schematically depicted in Fig. 2.4. Indicating with N_A the number of available amplifiers, the procedure can be schematized as follow:

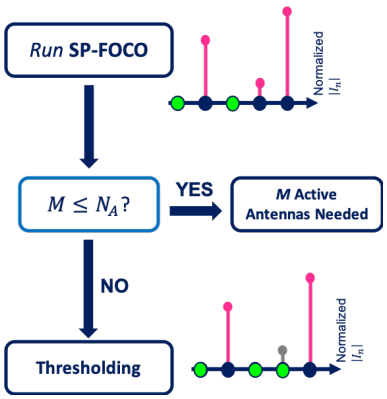

Fig. 2.4. Schematic view of the proposed SP-FOCO. M indicates the number of active elements identified by SP-FOCO and N_A the desired number of active elements, i.e., the number of available amplifiers

1. The complex excitations coefficients I_n are determined through the proposed SP-FOCO;
2. Evaluation of M: the number of excitation coefficients different from zero;
3. If $M \leq N_A$: M antennas can be exploited in the treatment;
4. If $M > N_A$: a thresholding procedure is applied [67];

In case the number of active antennas is larger the available amplifiers, i.e., $M > N_A$, our thresholding procedure aims at setting to 0 the $M - N_A$ antennas exhibiting lower weights in terms of $|I_n|$, as schematically depicted in Fig 2.4.

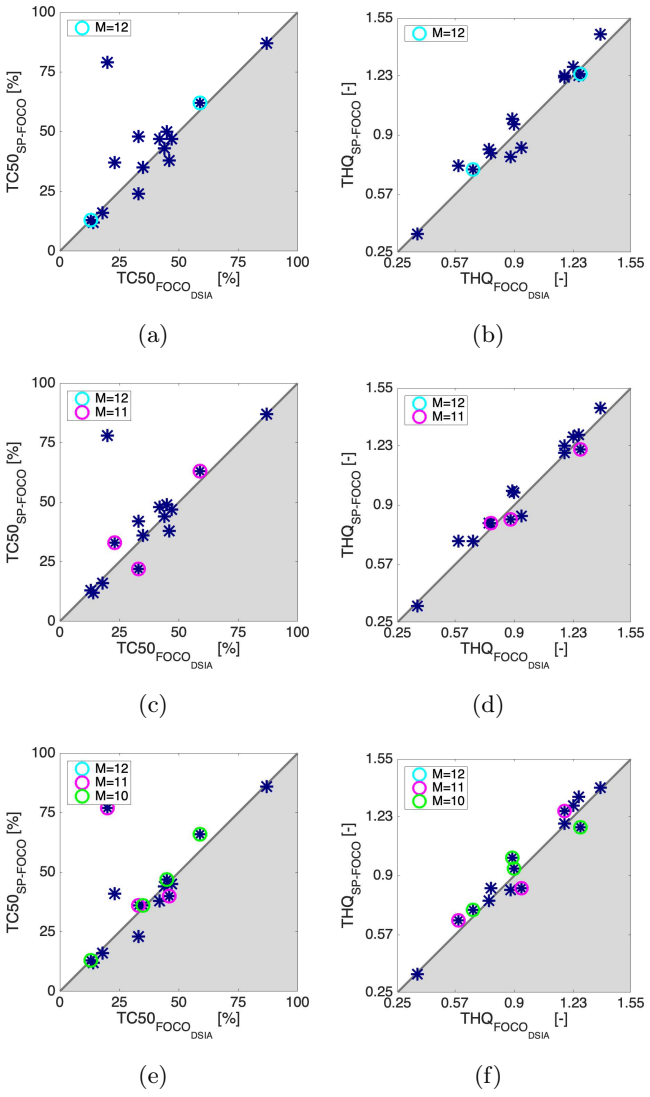

Fig. 2.5. Comparison of SAR-based quality parameter achieved with SP-FOCO and FOCO_{DSIA} on TC50 (1st column) and THQ (2nd column) concerning ϵ_1 (1st row),ϵ_2 (2nd row) and ϵ_3 (3rd row). Cases where $M = 12$, $M = 11$ or $M = 10$ are marked with additional light blue, pink and green circles, respectively.

2.2.2 Evaluation Setup

The considered dataset consists of fifteen 3D patient models generated during HTP for patients with H&N cancer that were planned for treatment with the HYPERcollar3D and as from Sect. 1.3.

In order to quantitatively evaluate the proposed approach, the SAR pattern was optimized through both SP-FOCO and FOCO exploiting the antenna selection procedur presently adopted at the Erasmus MC, where a selection procedure has been devised for the HYPERcollar3D applicator [40]. This applicator consists of a ring-shaped phased array made up by twenty patch antennas. Since twelve amplifiers are available, twelve out of the whole available array elements are selected individually for each patient. The clinical antenna selection approach identifies antenna-wise the twelve Dominant SAR Inducing Antennas (DSIA) within the HTV. This procedure, while being very intuitive, may suffer from the drawback of not exploiting interferences of the electromagnetic fields generated by different antenna subsets. As a matter of fact, destructive interference of fields generated from two antennas far from the HTV could counteract (or even avoid) hot-spot occurrence.

Different ϵ values have been tested. Accordingly, we considered $\epsilon_1 = 12/20\epsilon_{wa}$, $\epsilon_2 = 11/20\epsilon_{wa}$ and $\epsilon_3 = 10/20\epsilon_{wa}$. Here, ϵ_{wa} was evaluated as the $\|I_n^{wa}\|_{l_1}$ averaged on 15 patients where the I_n^{wa} have been obtained optimizing through FOCO when considering 20 antennas.

The comparison was carried out exploiting both SAR-based and temperature-based quality metrics as reported in Appendix A. Let us stress that these standard SAR-based quality metrics, implemented in the clinical tool VEDO, are used for clinical decision making and patient inclusion as they have been correlated to temperature-based quality metrics [29,70] which have been previously shown predictive for clinical outcome [22,29,58,71,72].

Finally, in order to quantitatively assess the impact of the thresholding procedure, the so-called thresholding error has been introduced and evaluated. Such a metric indicates the percentage of the truncated energy of the complex excitations, evaluated as the $\|\cdot\|_{l_2}$.

2.2.3 Results & Discussion

In this study, we have demonstrated the interest of SP-FOCO as an innovative approach for hyperthermia treatment planning, based on SAR constrained optimization via convex programming and the compressive sensing theory. The assessment has

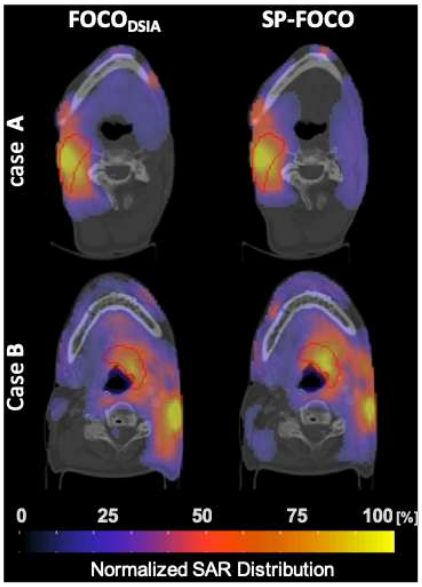

Fig. 2.6. Normalized SAR distribution related to case A and B on a axial view obtained by means of FOCO$_{DSIA}$ and SP-FOCO

been carried out in an actual clinical scenario and the outcomes compared to the clinically used antenna selection procedure, i.e., choosing as the dominant SAR inducing antennas [40]. The results showed that on average the proposed approach is able to outperform, although not by far, the adopted benchmark. Investigating various sparsity promoting parameter values, ϵ, had a twofold outcome: first, it helped setting the most suitable value of such parameter for the case at hand and, second, it suggested the proposed approach as an applicator design procedure, aimed at determining both the optimal number and position of radiating element starting from the patient data.

Figure 2.5 depicts the results obtained by means of both FOCO and SP-FOCO when adopting ϵ_1, ϵ_2 and ϵ_3. Each graph reports the comparison of one SAR-based quality metric. In each sub-graph, each star represents one patient. Hence, all the cases in which stars appear in the upper (white) triangle SP-FOCO is outperforming FOCO$_{DSIA}$. According to theory, by lowering the sparsity parameter the number of active elements was reduced. When exploiting ϵ_1, the procedure was able to identify two cases in which the number of active elements was exactly equal to the available amplifiers, i.e., M=12 - see Fig. 2.9. Surprisingly, when exploiting ϵ_2 and ϵ_1, the number of active elements in those cases is M=11 and M=10 which is lower to the available amplifiers - see Fig. 2.9. However, in the other cases where a soft thresholding procedure was applied, the truncation error was always found to be below 1%.

Interestingly, the antenna selection process pursued by the proposed SP-FOCO is never equal to the clinically adopted process, i.e., the DSIA ones. In particular, two different scenarios can be identified: the deep-seated HTVs and the one closer to the skin surface. Results related to one patient for each case, A and B, have been reported in Figs. 2.7 and 2.6. Here, we reported for both cases the $|I_n|$ obtained through FOCO_{DSIA} and SP-FOCO exploiting ϵ_1 and the induced SAR distributions. Clearly, in the first case, choosing the antennas inducing the average higher SAR in the HTV is a physically meaningfully procedure. However, while a different, still very similar, antenna subset are selected, results are approximately equal (only ΔTHQ was found $\approx +4\%$). On the other side, SP-FOCO improvements are more evident in the case of the deeper seated tumors. In reference to case B, indeed, both the active radiating elements and the resulting SAR pattern are very different ($\Delta T50 \approx +14\%$ and $\Delta THQ \approx +4\%$) - see Fig. 2.7 and 2.6.

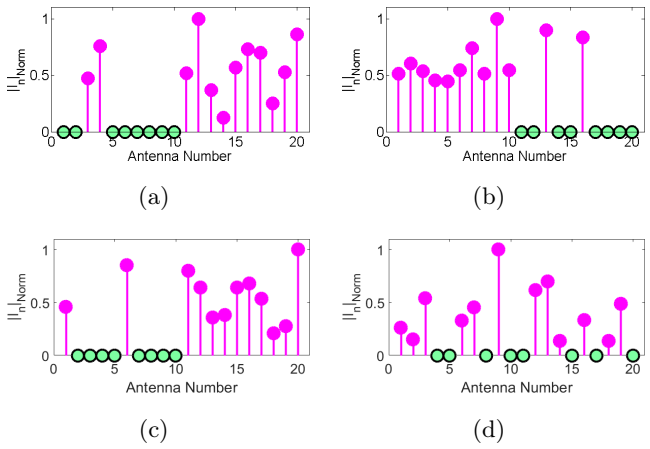

Fig. 2.7. Normalized excitation coefficients evaluated through SP-FOCO (1st row) and FOCO_{DSIA} (2nd row) for patient A and B, 1st and 2nd column, respectively.

When comparing FOCO with SP-FOCO results, on average, show a difference of 1% for TC25 and TC75. A more significant improvement has been observed for THQ ($\approx +4\%$) and for TC50 which, amongst all, was shown to be the most temperature predictive [70]. Improvements on TC50 equal to +6%, +5% and +4% were found when exploiting respectively ϵ_1, ϵ_2 and ϵ_3. These promising results proved the feasibility of exploiting the CS theory in HTP. However, there are few cases in which performances are not improved. This can probably be the price of considering the $\|\cdot\|_{l_1}$ rather than the (pseudo-) $\|\cdot\|_{l_0}$. According to the CS theory, in order to deal with sparse signals, one should consider the $\|\cdot\|_{l_p}$ where p should be as small as possible (but > 0) [73]. On

the other side, the set defined $\|\cdot\|_{l_p}$ is not convex as long as $p < 1$, so the optimization problem would be cast as a hard one [66, 73].

Finally, it is worth noting that in this feasibility study we decided not to assess performance of SP-FOCO as compared to the clinical optimization routine [11]. Here, indeed, one component of the field was assumed to be dominant amongst the others. In [74], we showed that within the HYPERCollar3D, the field component along the main axis of the patient is the dominant one by approximately a ratio of 3 ± 0.8. However, the clinical optimization routine, optimizes the SAR distribution taking into account the whole vector nature of the electric field. Hence, since field depolarization could be exploited towards a "more optimal" solution, in this feasibility study we avoided such a biased comparison. However, let us note that the extension to the case of vector field, while computationally more onerous, is straightforward following the guidelines in [63].

2.3 Multi-Frequency FOCO

The idea to adopt multi-frequency applicator was firstly proposed by Trefná et al. [42]. Then, in [34], multi-frequency-based HTP was introduced under the assumption that this could decrease undesired heating in healthy tissues [34]. Under the assumption that the collocation of undesired hot spots will change with frequency, one can possibly exploit this additional degree of freedom to lower the hot-spot occurrence outside the target volume. Notably, one does need wide-band antennas, as dual frequency or multi band antennas (which are widely diffused in the telecom applications) are sufficient. However, the procedure presented in [34], similarly to the TR-based one very recently proposed by Trefná et al. [75, 76], cannot guarantee the avoidance of such hot-spots.

In the following, starting from the FOCO theory and exploiting a multi-frequency applicator[4], an innovative multi-frequency approach, the multi-frequency FOCO (mf-FOCO) is herein detailed and discussed. Similarly to FOCO, this strategy allows to achieve a focused SAR distribution in correspondence of a given target point located within the tumor, while constraining the power distribution deposition elsewhere. In addition, by exploiting frequency diversity, it also allows achieving the maximum possible separation between the main SAR peak, in the target point, and the secondary hot-spot. Furthermore, by recurring to some simplifying still reasonable assumption, the proposed multi-frequency approach reduces to a CP problem and, as such, it delivers an *optimal* solution to the problem.

2.3.1 The proposed approach

With reference to the above described scenario, let us now consider the N elementary electric sources operating at different frequencies. In the following we dealt with scalar field and for sake of a cleaner notation we dropped the i, still referring with E to the dominant field component. Notably, hints on the extension to the case of vector fields are deferred to the conclusion. Hence, without loss of generality, let us initially deal with just two frequencies, say f_A and f_B, and let $E_A(\underline{r}) = \left|E_A(\underline{r})\right| e^{j\phi_A}$ and $E_B(\underline{r}) = \left|E_B(\underline{r})\right| e^{j\phi_B}$ be the corresponding steady state (phasor) fields at the two frequencies. Neglecting the beating terms giving a null contribution when averaging over the whole treatment duration, the overall SAR distribution in a generic point is given by:

$$SAR(\underline{r}) = \frac{1}{2}\frac{\sigma}{\rho}\left(\left|E_A(\underline{r})\right|^2 + \left|E_B(\underline{r})\right|^2\right) \tag{2.9}$$

where, by sake of simplicity, an average electric conductivity has been considered.

[4] We assume different excitations are used at the different frequencies.

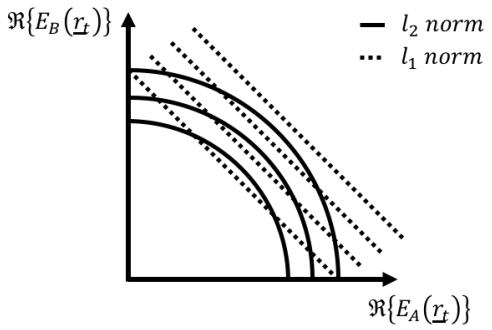

Fig. 2.8. Geometrical representation of the adopted relaxation. The l2 and l1 iso-norms, defined as the real part of the field in the target point at the two different frequencies, are sketched.

The multi-frequency focusing problem can be then formulated as:

Determine I_n^A *and* I_n^B $n = 1, 2, ..., N$ *such to:*

$$max\Big[\big|E_A(\underline{r}_t)\big|^2 + \big|E_B(\underline{r}_t)\big|^2\Big] \tag{2.10}$$

subject to:

$$\big|E_A(\underline{r})\big|^2 + \big|E_B(\underline{r})\big|^2 \leq UB(\underline{r}) \qquad \underline{r} \in \Omega \setminus \Pi(\underline{r}_t) \tag{2.11a}$$

Notably, eq. (2.9) holds true whatever the phase shift $\phi_A - \phi_B$. Hence, by using different excitations, say $\{I_n^A\}$ and $\{I_n^B\}$ at the two different frequencies, it is possible to set the phase reference ϕ_A and the phase shift $\phi_B - \phi_A$ in such a way that the corresponding phasor fields are both real and positive at the target point, allowing a significant simplification of the optimization problem. Consequently, the overall approach can be re-cast as:

Determine I_n^A *and* I_n^B $n = 1, 2, ..., N$ *such to:*

$$max\Big[\Big[\Re\{E_A(\underline{r}_t)\}\Big]^2 + \Big[\Re\{E_B(\underline{r}_t)\}\Big]^2\Big] \tag{2.12}$$

subject to:

$$\Im\{E_A(\underline{r}_t)\} = 0 \tag{2.13a}$$

$$\Im\{E_B(\underline{r}_t)\} = 0 \tag{2.13b}$$

$$\big|E_A(\underline{r})\big|^2 + \big|E_B(\underline{r})\big|^2 \leq UB(\underline{r}) \qquad \underline{r} \in \Omega \setminus \Pi(\underline{r}_t) \tag{2.13c}$$

This latter, while easier to be optimized as compared to problem (2.10-2.11a), is still a NP-hard problem. To circumvent this difficulty, let us suppose that the two frequencies contribute by a similar amount to the cost functional (2.10). Accordingly, we can conveniently introduce the relaxed functional:

$$max\Big[\Re\{E_A(\underline{r}_t)\} + \Re\{E_B(\underline{r}_t)\}\Big] \tag{2.14}$$

which is linear in the unknowns.

In fact, (see Fig. 2.8 for a better comprehension), as long as $\Re\{E_A(\underline{r}_t)\}/\Re\{E_B(\underline{r}_t)\} \approx 1$ the optimization of the l_2 norm (2.10) can be well approximated by optimization of the corresponding l_1 norm (2.14).

Finally, the resulting *linearly-relaxed* cost function (2.14), together with constraints (2.13a-2.13c), again allows one to deal with a CP problem which can deliver the globally optimal solution by means of off-the-shelf local optimization procedures.

Note that, to further improve performances, the globally optimal solution of problem (2.14, 2.13a-2.13c) can be possibly used as an *optimal-biased* initial guess for the original problem (2.12, 2.13a-2.13c).

The extension of the proposed mf-FOCO approach can be generalized to the case of more than two frequencies in an easy fashion. The extension to the case of vector fields, while conceptually straightforward, is instead more computationally cumbersome, as one also has to determine the optimal polarization for each single frequency. Such a strategy can be developed along the guidelines of [77, 78].

2.3.2 Preliminary Assessment

In this section we present the results of an extensive numerical campaign aimed at validating the proposed mf-FOCO as a promising tool in HTP.

In this thesis, the proposed approach has been tested as opposed to monochromatic FOCO and to a different multi-frequency procedure proposed in [19]. This latter consists in overlapping the focused SAR distribution gathered by means of the FOCO technique *independently* applied at the different frequencies. This simple scheme, from now on termed independent multi-frequency FOCO (i-mf-FOCO), while easy to be implemented, requires to solve a number of convex programming (CP) problems equal to the number of frequencies and it still does not allow to guarantee any constraint on the power deposition outside the target area.

In the following, after a description of the numerical test bed, we reported the results of our analysis in terms of SAR and temperature distribution.

The adopted numerical test bed

The test-bed used in this study is made up by 2-D breast phantoms derived from the anatomically and electromagnetically realistic 3-D phantoms provided by Wisconsin repository [79]. The phantoms are representative of four virtual patients characterized

by fatty, scattered fibroglandular, heterogeneously dense, and very dense breast compositions. They are, respectively named: Breast Class (BC) I fatty breast (slice 155 - phantom ID:071904); BC II scattered fibroglandular breast (slice 158 - phantom ID:012204); BC III heterogeneously dense breast (slice 100 - phantom ID:080304) and BC IV very dense breast (slice 100 - phantom ID:012304).

The original phantoms are referred to healthy patients and therefore a circular inclusion, of radius $\approx 0.5cm$, simulating a tumor has been inserted in the breast model. In order to cover all the realistic possibilities, for each phantom two different tumor positions have been considered: an intra-glandular tumor and an extra-glandular one. Tumor dielectric properties have been set accordingly to the literature adopting a single-pole Debye dispersion characteristic [80].

The breast is supposed to be surrounded by a matching and/or cooling liquid aimed at both reducing the reflection at the breast surface and keeping the skin temperature curbed. Following [81,82], the relative permittivity and the conductivity of such a background medium have been set equal to 18 and $0.1S/m$, respectively. Note such a background medium can be realized by proper mixtures of Triton-X and water. Triton-X is a safely handling non-ionic detergent, so that it can be actually used to obtain the background medium permittivity as in the simulations.

The applicator is supposed to be a circular array of elementary (filamentary) currents surrounding the breast phantom with a radius $\approx 14cm$. The number of array elements, N, has been determined according to the theory of Degrees of Freedom (DoF), [52,64], in order to provide optimal performances while not being redundant. In the following numerical examples, performed at $f_A = 1.25GHz$ and $f_B = 1.75GHz$, the number of array elements has been set as the *average* of the degrees of freedom related to each frequency, respectively equal to $N \approx 2\beta a$, where $\beta = 2\pi/\lambda$ is the real part of the wave number in the background medium and a is the radius of the minimum circle enclosing the region to be treated. Thus, considering an average breast dimension of $\approx 7cm$, N has been set equal to 28. Note that f_A and f_B have been chosen, following [19], on the basis of a trade-off between penetration depth and resolution.

Electromagnetic Focusing: Results Analysis

By sake of brevity, Fig. 2.9 depicts some of the normalized SAR distributions achieved by means of mf-FOCO at $f_A \cup f_B$ for both the intra- and extra-glandular case. As expected, the SAR distributions are peaked into the target point and the maximum hot-spot amplitude, even in the worst case, is kept below 31%. Notably, it drops of

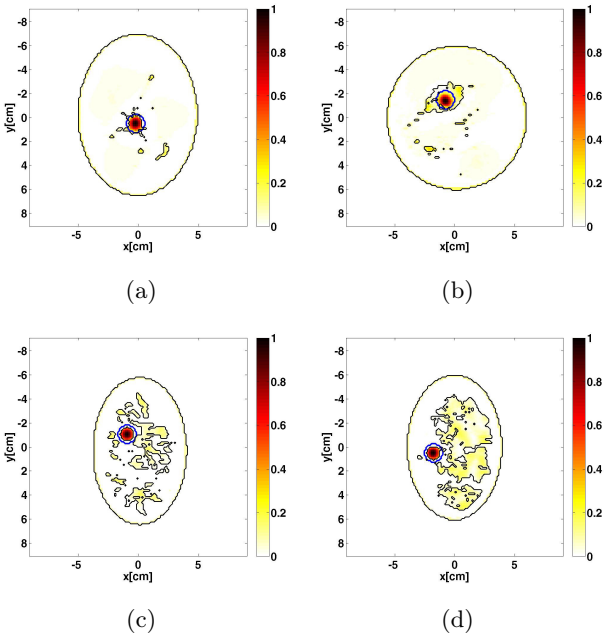

Fig. 2.9. Normalized SAR distribution achieved with the proposed mf-FOCO exploiting f_A and f_B. Intra-glandular tumor case (1^{st} row) is reported for fatty and scattered fibroglandular breast (a and b, respectively) whereas the extra-glandular tumor case (2^{rd} row) for heterogeneously dense and very dense breast (c and d, respectively). Breast shapes and target area contours are reported by black and blue lines, respectively.

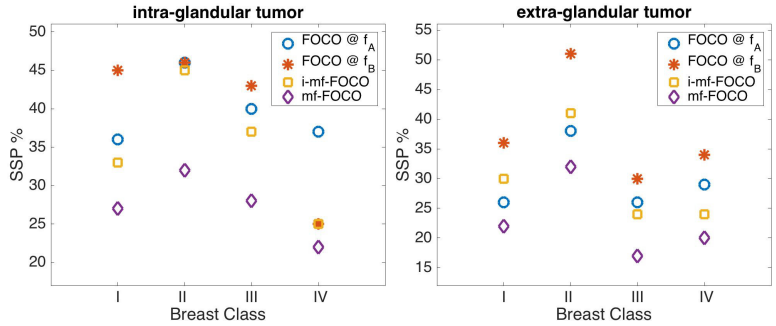

Fig. 2.10. Maximum SAR side peak obtained by means of monochromatic FOCO at f_a and f_b (green and light blue dashed line, respectively), i-mf-FOCO and mf-FOCO at f_a+f_b (yellow and dark blue dashed line, respectively) for both intra-glandular (a) and extra-glandular (b) tumors.

$\approx 10-15\%$ on average with respect to monochromatic FOCO or i-mf-FOCO. Note that the mask function herein adopted has been *ad-hoc* tailored on the requirements of each specific case. In particular, a difference equal to $-3dB$ has been set between adipose an fibroglandular tissue to counteract the higher losses exhibited by this lat-

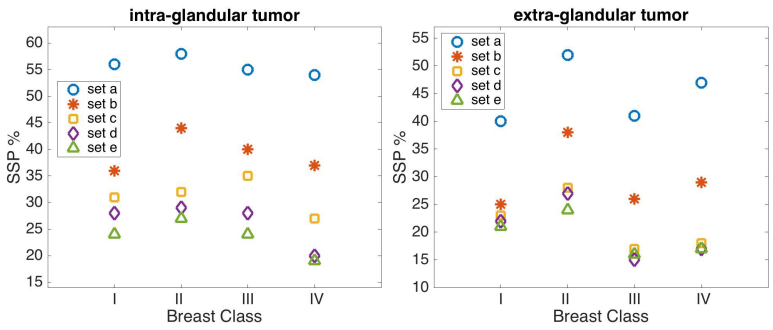

Fig. 2.11. Maximum SAR side peak obtained by means of the proposed mf-FOCO exploiting from 1 (set a) to 5 (set e) frequencies in the range $1-2GHz$ (with a step equal to $250MHz$) for both intra-glandular (a) and extra-glandular (b) tumors.

ter. A performance comparison between mf-FOCO and both monochromatic FOCO and i-mf-FOCO has been carried out. In particular, the different normalized SAR distributions have been compared. In Fig. 2.10, we report the maximum hot-spot amplitude for all the considered cases. The results confirm the optimality of the SAR distribution (in terms of minimal hot-spot) achieved by means of the proposed technique. In a restricted number of cases the i-mf-FOCO exhibits good performances, but it cannot avoid undesired SAR peaks.

The second goal of this study was aimed at assessing the effect of using more than just two frequencies. To this end, different frequencies sets have been considered in the frequency range $[1-2]GHz$. Starting $f = 1GHz$, set a, we progressively increase number of frequencies with a $250MHz$ step, until we reach $2GHz$ (set e, 5 frequencies). The number of sources adopted for this study has been kept constant and equal to 28. The results of such analysis are depicted in Fig. 2.11, where we report the hot-spot amplitude obtained with mf-FOCO for all the considered cases (i.e. breast class/tumor position). Notably, the possibility of decreasing the hot-spot prominence by exploiting frequency diversity is bounded. A saturation type trend can be, indeed, identified since no meaningful improvement can be achieved with more than 3 frequencies. Of course, the choice of the working frequencies plays a relevant role. However, in view of the initial aims of the study, such a point is not further developed herein.

Thermal Focusing: Results Analysis

The thermal distributions corresponding to the above cases and solutions have been obtained by solving the Pennes' Bioheat Transfer equation [53]. The thermal problem

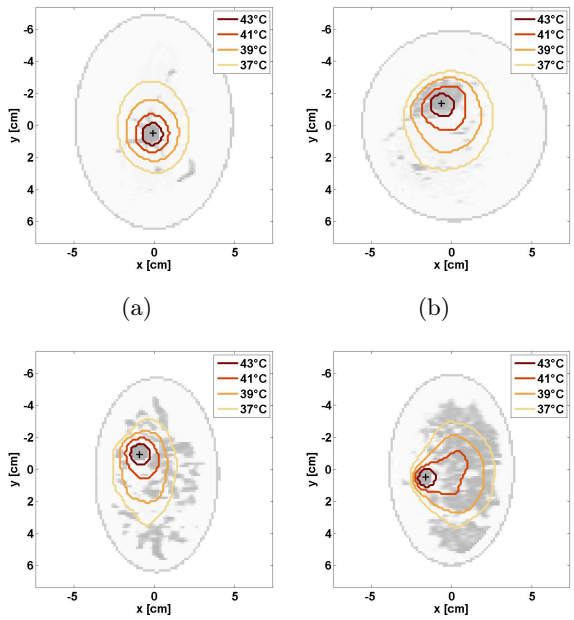

Fig. 2.12. Temperature distribution corresponding to the SAR distribution shown in Fig. 2.9. Intra-glandular tumor case (1^{st} row) are reported for fatty and scattered fibroglandular breast (a and b, respectively). Extra-glandular tumor case (2^{rd} row) are reported for heterogeneously dense and very dense breast (c and d, respectively). Breast shapes and anatomical structure are reported in gray.

has been numerically solved by means of the Comsol Multiphysics BioHeat Transfer Module exploiting the typical average values for breast tissues [79, 83], as reported in [19], and considering a $50 - min$ treatment [5, 19]. The effect of the cooling ($15°C$) medium on the skin has been modeled by imposing convective boundary conditions with a convective coefficient of $300W/m^2K$ [83]. The heating potential, entry of the Pennes' Bioheat Transfer equation, has been empirically determined in such a way to achieve a temperature at the desired focus, $\underline{r}_t$, of $\approx 45°C$ [19]. Note that this operation simply corresponds to scaling the antenna excitations, i.e. $\{I_n\}$, so that the achieved temperature distribution corresponds to the appropriately scaled array excitation set.

For the sake of comparison the thermal analysis has been conducted by exploiting the above mentioned monochromatic and multi-frequency approaches considering both an intra- and an extra-glandular tumor for all the different BCs. Figure 2.12 depicts the temperature distribution, obtained by means of the proposed mf-FOCO approach at $f_A \cup f_B$, related to the SAR distributions as shown in Fig. 2.9. To better appreciate from a visual point of view the resulting temperature distribution, different iso-temperature contours at $43, 41, 39$ and $37°C$ have been visualized with the

Table 2.3. Thermal Focusing Performances: Intra-Glandular Tumor Case

	TA $[cm^2]$				**UHA** $[cm^2]$				**TBPT** $[^\circ C]$			
Technique\BC	I	II	III	IV	I	II	III	IV	I	II	III	IV
FOCO@f_A	1.5	2.1	1.3	1.9	3.8	6.5	3.8	7.7	45.4	45.4	45.2	45.6
FOCO@f_B	2.1	2.11	2.1	1.2	7.3	8.1	6.1	4.8	45.5	45.3	45.5	45.6
i-mf-FOCO	1.8	2.0	1.7	1.6	4.8	7.1	5.3	6.0	45.5	45.3	45.6	45.6
mf-FOCO	1.3	1.6	1.2	1.1	3.9	6.0	4.0	4.6	45.1	45.2	45.1	45.1

Table 2.4. Thermal Focusing Performances: Extra-Glandular Tumor Case

	TA $[cm^2]$				**UHA** $[cm^2]$				**TBPT** $[^\circ C]$			
Technique\BC	I	II	III	IV	I	II	III	IV	I	II	III	IV
FOCO@f_A	1.5	1.3	1.1	1.1	3.7	5.1	2.4	3.3	45.8	45.3	45.6	45.5
FOCO@f_B	1.4	1.3	1.0	3.2	5.4	9.9	3.5	13.2	45.4	45.2	45.2	45.1
i-mf-FOCO	1.3	1.6	1.0	1.1	4.0	6.8	2.7	6.5	45.2	45.6	45.4	45.3
mf-FOCO	1.2	1.2	1.2	1.0	3.5	5.8	4.0	6.0	45.1	45.1	45.1	45.0

related breast anatomical map. The peak temperature locations are marked with a black cross.

Results show that the technique is both able to deliver a temperature focused into the target point and able to be very selective. The therapeutic temperature is achieved in an area surrounding the target point not larger than $\approx 1.5cm^2$, in agreement with surgical resection protocols [84, 85].

The effectiveness of the obtained thermal distributions has been analyzed and compared by exploiting the following synthetic parameters:

- Treated Area (TA), defined as the area of the breast where the temperature reaches values higher than the therapeutic value ($43^\circ C$);
- Undesired Heated Area (UHA) defined as the area of the healthy breast where the temperature reaches values higher than $41^\circ C$;
- Tumor Breast Peak Temperature (TBPT) defined as the highest temperature reached in malignant breast tissues -TBPT $\approx 45^\circ C$;

Tables 2.3 and 2.4 reports the overall thermal analysis in terms of the above described metrics. All the investigated single/multi-frequency focusing strategies are able to achieve a temperature distribution focused into the target point and mf-FOCO outperforms the other methods in terms of TA. In some cases, one also notices an increased UHA for mf-FOCO. Such a circumstance can be attributed to the fact that

the final temperature distribution depends not only from hot-spot, but also from the overall SAR distribution as well as on the specific thermal parameters of the different tissues. We expect in fact that an even better temperature control can be achieved by using a $UB(\underline{r})$ mask such to take into account both the e.m. and thermal parameters of the different tissues.

3

Un-Constrained Power Shaping

In this Chapter we propose a novel un-constrained optimization approach aimed at shaping the power deposition uniformly over an extend target area, as in Fig. 1.2.(b), or in a multi-spot focused fashion, see Fig. 1.2.(c). Probably because of the intrinsic challenging nature of the problem, while several focusing approaches have been proposed, only a few able to address this more demanding need can be found in the literature.

A shaped pattern can be possibily conceived as a superposition of many patterns focused in different points, named control points, set in the target volume. Hence a straightforward possibility would suggest to tackle the shaping problem by simply solving some focusing problems and then juxtapose the results. This strategy allows to control to some extent the field intensity through a proper choice of the distance among the control points. As an example, Zhao et al. [86] proposed a very simple shaping strategy, named independent multi target TR (i-mt-TR) which amounts to add the contributes gathered by solving, through TR, several focusing problems into different control points placed within a certain target area.

However, an additional degrees of freedom of the problem could be exploited. Surprisingly, indeed, when simply adding focused field intensity distributions one is neglecting the additional degrees of freedom represented by the phase shifts of the field in the different control points. Motivated by the lack in the literature of methods such to be both computationally and practically efficient, we propose in the following a shaping procedures exploiting this additional degree of freedom: the multi-target TR based on the (un-constrained) TR. In particular, starting from shaping state-of-the-art idea and noticing that this corresponds to exploit *in-phase* focused fields in the different control points, the developed procedures propose a more effective (still very simple) strategy, based on the same basic bricks. This allows to improve performance and to achieve a results in cases where a simple superposition fails. The basic idea of the techniques proposed in the following is that one can combine the

fields and excitations of the single target problems in a different fashion. In particular, the proposed procedure simply explores different phase shifts among the excitations of the single target problems. Then, observation of the performances achieved by the different superpositions will allow to *a-posteriori* determine the one leading to some "optimal" field intensity distribution.

In the remaining of this Chapter the proposed mt-TR is described and presented together with results achieved in a canonical scenario. Besides presenting the mt-TR, a twofold numerical assessment is provided. First, the analysis allows evaluating both the actual improvements with respect to state-of-the-art. Second, one can get a preliminary and empirical understanding of the more appropriate choice of the control points in order to shape (*uniformly* within a certain area either in a *multi-spot focused* configuration) the field intensity within a 3-D in-homogeneous scenario.

3.1 Multi-Target Time Reversal

The procedure herein proposed is similar in spirit to both the one proposed by Zhao et al [86] it exploits the same additional degree of freedom so far surprisingly neglected. In the following, we dealt with scalar field and for sake of a cleaner notation the i indicating the dominant component has been dropped.

Considering the same general framework described at the beginning of Chapter I, let us consider a set of control points ($\underline{r}_{tk}$ $(k = 1, .., L)$) arbitrary located into the target area. Denoting with $\Psi_n(\underline{r}_{tk})$ the total field measured by the n-th antenna when a unit amplitude point source is located into the control point $\underline{r}_{tk}$, according to the standard TR theory, the focused (time-reversed) field in $\underline{r}_{tk}$ is provided by:

$$E_k(\underline{r}) = \sum_{n=1}^{N} \Psi_n^*(\underline{r}_{tk}) \Phi_n(\underline{r}) \tag{3.1}$$

where $*$ denotes the conjugation operation.

A first "basic" shaping approach is the so-called i-mt-TR [86] and it is cast as a simple sum of the excitations corresponding to different control points, so that:

$$E(\underline{r}) = \sum_{n=1}^{N} \sum_{k=1}^{L} \Psi_n^*(\underline{r}_{tk}) \Phi_n(\underline{r}) \tag{3.2}$$

which simply corresponds to sum the excitations related to the different focusing problem.

By the sake of simplicity, let us refer to the case of just two control points and let $\phi_1 \in [0, 2\pi]$ be an auxiliary variable indicating the phase shift between the fields in $\underline{r}_{t1}$ and $\underline{r}_{t2}$ (as computed from single target TR).

As such, the mt-TR approach, for each (sampled) value of ϕ_1, casts the shaping problem as the combination (through complex unit amplitude coefficients) of the fields focused in correspondence of $\underline{r}_{t1}$ and $\underline{r}_{t2}$ through TR. The excitations coefficients could be determined as:

$$I_n = \Psi_n^*(\underline{r}_{t1}) + \Psi_n^*(\underline{r}_{t2}) e^{j\phi_1} \tag{3.3}$$

where ϕ_1 is another degree of freedom of the problem.

In case L control points are considered, if we indicate with $\boldsymbol{\phi} = \{\phi_k\}_{k=1,..,L-1}$ the vector containing the $L-1$ auxiliary variables having the physical meaning of the phase shift between the field at the "reference" control point $\underline{r}_{t1}$ and the k-th control point, i.e., $\underline{r}_{tk}$, eq. (3.3) will become:

$$I_n(\boldsymbol{\phi}) = \Psi_n^*(\underline{r}_{t1}) + \sum_{k=1}^{L-1} \Psi_n^*(\underline{r}_{tk}) e^{j\phi_i} \tag{3.4}$$

Of course, a key point is how to select the optimal phase shifts. This requires two ingredients: the definition of an objective function and the application of some optimization criterion. In all cases where just a few control points can be considered the optimal solution can be determined enumeratively observing a-posteriori the results achieved at the different $\boldsymbol{\phi}$ values, and picking the most convenient one according with the application at hand.

The generalization to the case of L control points and M sampled values of the auxiliary variables will require M^{L-1} linear superposition, thus impacting the computational burden (which could eventually take advantage from parallel computing).

A possible goal is to maximize the field intensity in the considered shaped region, in this thesis the average field intensity in the target volume, indicated as $\Pi(\underline{r})$, was considered to be the objective function.

In particular, the "optimal" phase shifts are selected as:

$$\max_{\boldsymbol{\phi}} \int_{\Pi(\underline{r})} \left|E(\underline{r})\right|^2 d\underline{r} = \int_{\Pi(\underline{r})} \left| \sum_{n=1}^{N} I_n(\boldsymbol{\phi}) \Phi_n(\underline{r}) \right|^2 d\underline{r} \tag{3.5}$$

where $I_n(\boldsymbol{\phi})$ are as from eq. (3.4).

Another possibility could, for instance, consist in selecting amongst the different $\boldsymbol{\phi}-$solutions the one providing the best trade off between the field intensity uniformity within the target area and the lowest side peak elsewhere. This latter could result of interest for the case of microwave hyperthermia. Of course, very many different choices are possible for the objective function as well as for the a-posteriori criterion for the selection of the "optimal" phase shift, and more sophisticated methods will be required for optimization when considering more control points. However, as our main aim here is to demonstrate the usefulness of the additional degrees of freedom we have introduced, both these points (where many possible alternatives can be fruitfully introduced) are outside of the scope of this thesis.

Note, the approach can be eventually extended to the case of a non-uniform shaping by inserting a given amplitude factor. The extension to the vector case can be pursued by following the guidelines implemented in [77, 78].

3.1.1 Assessment in 3-D inhomogeneous scenario

The 3-D scenario used for the validation is depicted in Fig. 3.1.(a) and consists in two dielectric objects (a cube and a sphere) contained in a spherical region of interest, i.e. Ω, which is hosted in free space. The diameter of Ω is $d_\Omega = 2,5\lambda_m$[1] and its relative

[1] Being λ_m the wavelength in the background medium

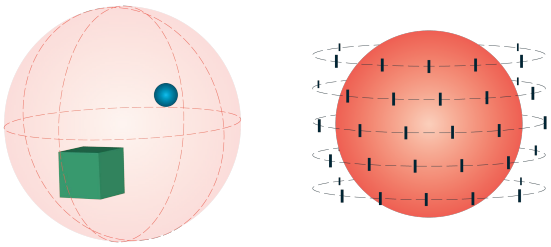

(a) (b)

Fig. 3.1. Scenario used for validation (a) and antenna array configuration (b).

Table 3.1. Details on control points and target area for the tested numerical configurations.

Conf.	**Control Points**		**Target Area**		
	#	*Distance*	*Shape*	*Dimension*	*Axes*
0	2	$0.4\lambda_m$	-	-	x
I	3	$0.4\lambda_m$	Ellipsoid	$1.5 \times 0.3 \times 0.3\lambda_m$	z
II					z-y
III	2	$0.4 \div 2\lambda_m$			x-y
IV	3	$0.4\lambda_m$	Spheres	$0.3 \times 0.3 \times 0.3\lambda_m$	y
V		$0.65\lambda_m$			x

permittivity equal to $\epsilon_\Omega = 2$, the cube has a side of $l_c = \lambda_m/2$ and $\epsilon_c = 4$, whereas the sphere has a diameter of $d_s = \lambda_m/4$ and $\epsilon_s = 3$.

The antennas array is cylindrical array of radius $r \approx 2\lambda_m$ made up by 65 very small unitary-excited dipoles, arranged over 5 equi-spaced circles, along the z-axis (i.e., 13 per circle), as shown in Fig. 3.1.(b). Numerical simulations have been performed using a 3-D full wave finite element solver with a working frequency of $1.5GHz$. Finally, only the *z-component* of the field has been optimized since, according to the considered antennas configuration, this component can be considered to be dominant above the others.

The following analysis is articulated in three different numerical experiments whose details are reported in Table 3.1. First, the different possible impacts of the phase shifts values is discussed and emphasized. To this end, two control points have been placed along the x-axis at a distance of approximately $0.4\lambda_m$, say configuration 0 - see Table 3.1. Then, excitations (4) have been determined for with different ϕ values, and the resulting $\boldsymbol{\phi}-$solutions observed. In this starting example, as well as in the other numerical experiments, 20 values of ϕ have been uniformly sampled between 0 and 2π.

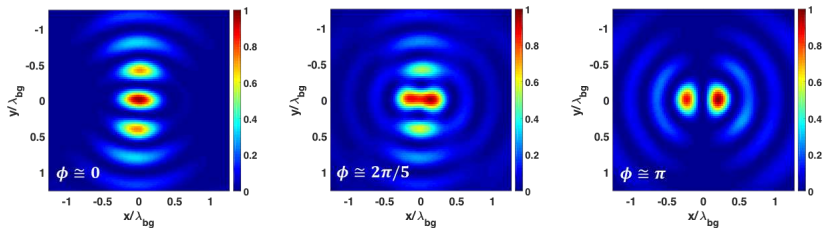

(a) (b) (c)

Fig. 3.2. Squared field intensity distributions configuration 0 along a cut view on the x-y plane obtained by means of the i-mt-TR for $\phi = 0$ (a), $2\pi/5$ (b) and π (c). Control points set at $\approx 0.4\lambda_m$.

Second, we have tested the capability of the proposed approach to achieve a (nearly) uniform shaping of the field intensity over an extended target area. To this end, an extended ellipsoidal shaped target volume, of axes $\approx 3\lambda_m/2 \times \lambda_m/3 \times \lambda_m/3$, has been placed in two different positions[2] in Ω (configurations **I** and **II** in the following - see Table 3.1). In order to get the desired shaping, three control points have been used and arranged uniformly (with a spacing of $\approx 0.4\lambda_m$) along a segment placed in the center of mass of the target volume. In order to better (and quantitatively) appreciate the differences with respect to i-mt-TR, results have been appraised in terms of coverage factor (CF). The CF is defined as the fraction of the target area in which $\left|E(\underline{r})\right|^2$ is higher than 50% of its maximum value[3]. Such a parameter was adopted as an additional quality metric since it provides indications on how the field intensity is distributed within the target volume.

Third, we have proved the capability of the proposed approach to achieve a multi-spot field intensity distribution even in case of sub-wavelength spots spacing (which is unfeasible with i-mt-TR). To this end, two control points have been placed at a distance varying from $\approx 0.4\lambda_m$ to $\approx 2\lambda_m$ along the x- and the y-axes, indicated as configuration III - see Table 3.1. Then, the mt-TR and the i-mt-TR have been applied and compared.

Finally, in order to validate the approach for an even more difficult case, two different configurations (say **IV** and **V**) with three control points have been considered. In these latter examples the control points have been set at a distance approximately equal to $0.4\lambda_m$ and $0.65\lambda_m$ from the central point along the y- and x-axes, respectively indicated as configuration IV and V - see Table 3.1. Concerning this third analysis, dealing with the "multi-spots" field intensity shaping, the target volumes have been

[2] With the main dimension oriented along the z-axis.
[3] Ideally CF=1.

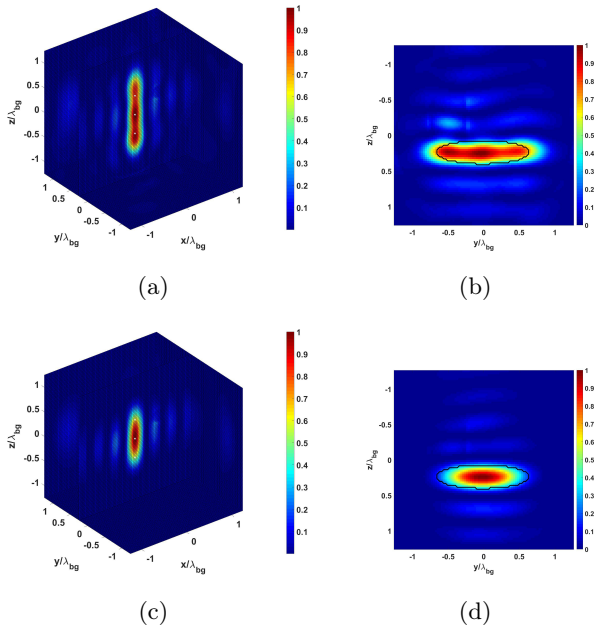

(a) (b)

(c) (d)

Fig. 3.3. Squared field intensity distributions for uniformly shaping obtained by means of mt-TR (a-b) and i-mt-TR (c-d) for configuration I in a 3D plot (a-c) and a cut view along the main axes of the target area (b-d). Target area is as black line and control points are as white dots.

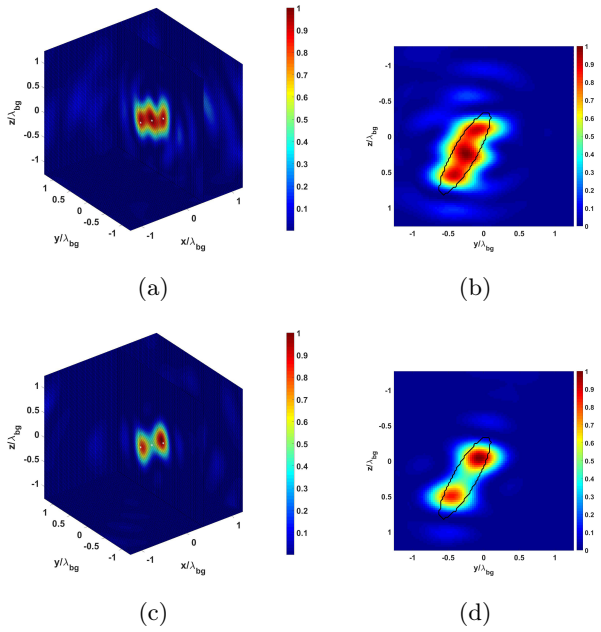

(a) (b)

(c) (d)

Fig. 3.4. Squared field intensity distributions for uniformly shaping obtained by means of mt-TR (a-b) and i-mt-TR (c-d) for configuration II in a 3D plot (a-c) and a cut view along the main axes of the target area (b-d). Target area is as black line and control points are as white dots.

modeled as spheres of diameters $\approx \lambda_m/3$ centered in the control points[4] [64,87]. Note that also in this last analysis, the CF has been observed in order to better estimate the performances of the two TR-based approaches.

Results: Analysis & Discussion

As a first result helping to understand the role of the auxiliary parameter ϕ, Fig. 3.2 depicts three $\boldsymbol{\phi}-$solutions, related to configuration 0. As it can be seen, different choices of the additional parameter allow to pass from a kind of shaped intensity (see Fig. 3.2.(b)) to a dual-spot configuration (see Fig. 3.2.(c)). In the same graph, Fig. 3.2.(a) represents the i-mt-TR, as in [86].

As far as the possibility to achieve uniformly shaped field intensities is concerned, Fig. 3.3-3.4 depicts the normalized squared amplitude of the fields obtained by means of mt-TR for both configurations **I** and **II**. In addition to what can be visually appreciated from a quantitative point of view, mt-TR is able to significantly enhance the uniformity of the field intensity within the target region with respect to mt-TR. In fact, for configuration **I**, the CF increases from 44% to 71%, whereas for configuration **II** it raises from 39% to 81%. Note that the proposed approach not only outperforms the original mt-TR in terms of CF, but in some cases, e.g., configuration **II**, is able to gather an uniform coverage of the target area which cannot be achieved at all by means of mt-TR (see Fig. 3.3.(d)-3.4.(d)).

As far as the multi-spot case is concerned, Fig. 3.5 depicts the CFs related to both mt-TR and i-mt-TR for the dual-spot focusing configuration III (i.e., along the x- and y-axes) as a function of the control points distance. From this plot, two different kind of results can be identified depending on whether the spacing is below or besides a threshold of approximately $0,8\lambda_m$. While for more "distant" control points an average improvement on CF of $\approx 10\%$ can be achieved, when the control points distance is smaller than $\approx 0.8\lambda_m$, mt-TR outperforms the i-mt-TR on average by 20% (and up to $\approx 45\%$). Similarly to the previous analysis, mt-TR is not only able to improve i-mt-TR performances, but it is also delivers a dual-spot focused field intensity distribution where the un-optimized approach fails, as shown in Fig. 3.6. More in detail, Fig. 3.6 depicts a cut view along the target areas of the normalized squared amplitude of the field obtained by means of mt-TR and O-mt-TR when target points are distant $\approx 0.5\lambda_m$.

[4] These analyses were not conducted along the z-axis as the cylindrical array configuration, while being realistic, does not allow a tight control of the field in this dimension.

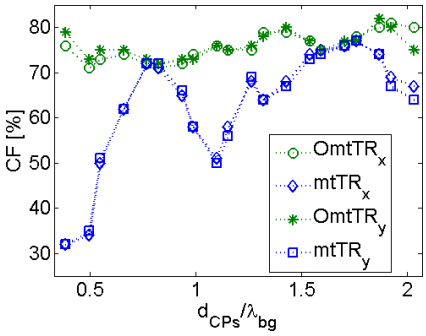

Fig. 3.5. Coverage factor obtained in configuration III by means of i-mt-TR and mt-TR with respect to control points distance for two control points along the x and the y axes respectively depicted in green (circle and stars) and blue (rhombus and squares).

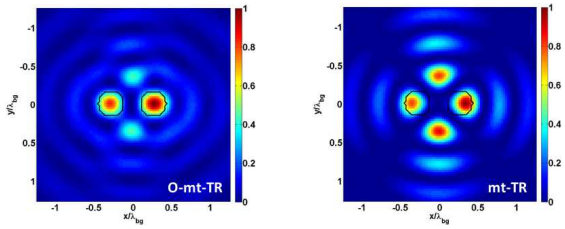

(a) (b)

Fig. 3.6. Squared field intensity distributions for multi-spot focusing obtained by means of mt-TR (a) and i-mt-TR (b) for configuration III with control points at $\approx 0.5\lambda_m$ in a cut view along the main axes of the target area. Target area is as black line.

Similar reasonings and performances can be observed in the three control points configuration IV and V. In these cases, indeed, as shown in Fig. 3.7 and 3.8, the CF is increased from 38% to 77% for configuration **IV** and similarly from 35% to 79% for configuration **V**. Apart from the metrics, which confirm the remarkable improvement, it is worth to note that in case of multi-spot focusing the mt-TR comes to be fundamental as the standard approach completely fails - see Fig. 3.7.(d)-3.8.(d).

From these results we can conclude that the auxiliary parameters represented by the phase shifts between the field in the different control points plays a role which is more and more relevant as the control point distance became smaller. As a matter of fact, when dealing with "distant" control points and multi-spot requirements, the additional degrees of freedom, while still relevant, are not necessary to avoid the failure of the field intensity control. Conversely, controlling the phase shifts becomes essential to deliver either a *uniformly* shaped or sub-wavelength *multi-spot* focused field intensity distribution when control point are at a sub-wavelength distance. This is likely the case of hyperthermia treatment planning. However, a constrained approach

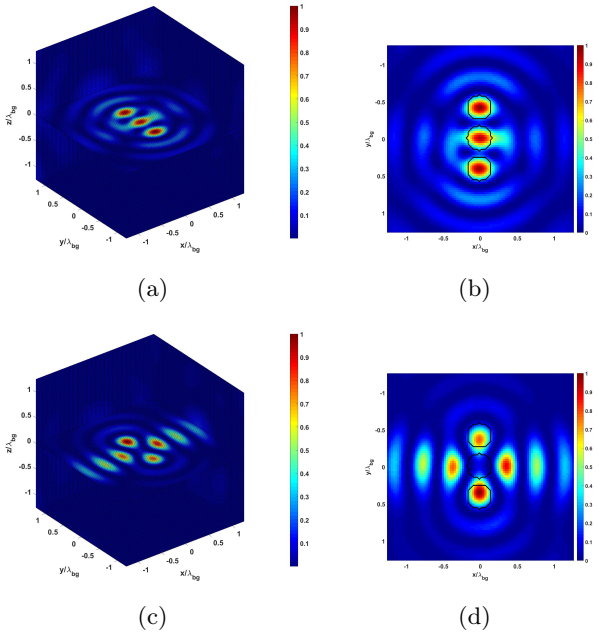

(a) (b)

(c) (d)

Fig. 3.7. Squared field intensity distributions for multi-spot focusing obtained by means of mt-TR (a-b) and i-mt-TR (c-d) for configuration IV with control points at $\approx 0.4\lambda_m$ in a 3D plot (a-c) and a cut view along the main axes of the target area (b-d). Target area is as black line and control points are as white dots.

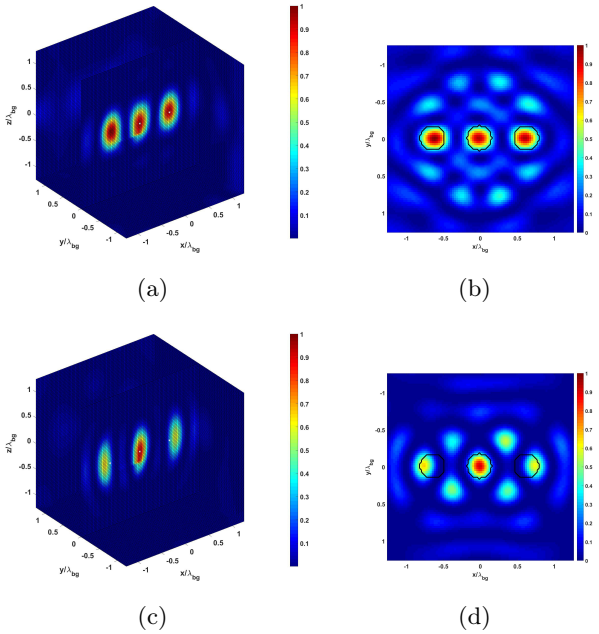

(a) (b)

(c) (d)

Fig. 3.8. Squared field intensity distributions for multi-spot focusing obtained by means of mt-TR (a-b) and i-mt-TR (c-d) for configuration V with control points at $\approx 0.65\lambda_m$in a 3D plot (a-c) and a cut view along the main axes of the target area (b-d). Target area is as black line and control points are as white dots.

able to arbitrary shape the field intensity distribution would be advisable to also ensure the avoidance of undesired heating.

Lastly we compared the computational burden of the proposed mt-TR as compared to the i-mt-TR. In our numerical experiments, we found that mt-TR delivers an increased computational time which passes from $\approx 0,17sec$ with i-mt-TR to $\approx 4,76sec$, for the case of two control points, and to $\approx 84sec$ for the case of three control points. All numerical calculation were run on a workstation equipped with two Intel Xeon E5-2687W processors and 256GB RAM.

4

Constrained Power Shaping

In this Chapter, the innovative constrained optimization routine, multi-target FOCO (mt-FOCO), has been proposed. The proposed approach is based on the homonym technique FOCO from which it inherited both the convex programming formulation and the possibility of enforcing hot-spot limiting constraints. Similarly to mt-TR (presented in the previous Chapter), also mt-FOCO is based on both the use of a number of control points, rather than just one target point, and of the additional degrees of freedom played by the phase shift of the field at the different control points.

Despite aimed at a common end, different aspects are singularly characterizing the mt-TR to the proposed mt-FOCO. From one side, mt-FOCO delivers the globally optimal solution by means of off-the-shelfs search algorithms as it casts the shaping problem as several CP problems[1]. On the other side, mt-TR is not able to enforce constrains on the power deposition outside the target area, as this represents an intrinsic limitation of TR, but it has a relatively modest computational burden since it "only" requires a linear superpositions for each considered phase shift value. Instead, analogously to FOCO, mt-FOCO exploits a mask function enabling *hot-spots* avoidance.

In the remaining of this Chapter the mt-FOCO is proposed and tested. First, its feasibility in a 3-D canonical scenario is reported and then, mt-FOCO is compared to the "standard" focusing FOCO in a preliminary clinical assessment.

[1] One for each considered phase shift value.

4.1 Multi-Target FOCO

Let us refer again to the general framework given at the beginning of Chapter I and consider the case one of the field components, $(E_i(\underline{r}))$, can be considered to be dominant above the other ones. Differently to mt-TR, herein the TR has been replaced by FOCO. Introducing $\underline{r}_{tk}$ $(k = 1, ..., L)$ as a set of "control points" located into the chosen target area and, for a better understanding, considering initially the case of $L = 2$, namely only $\underline{r}_{t1}$ and $\underline{r}_{t2}$, the problem of shaping the field intensity in a given target region, at a fixed frequency, can be formulated as:

Find I_n $(n = 1, ..., N)$ *such to:*

$$max\left\{ \sum_{k=1}^{2} \left[\Re\{E_i(\underline{r}_{tk})\}^2 + \Im\{E_i(\underline{r}_{tk})\}^2 \right] \right\} \tag{4.1}$$

subject to:

$$\left|E_i(\underline{r}_{t1})\right| = \left|E_i(\underline{r}_{t2})\right| \tag{4.2a}$$

$$\left|\mathbf{E}(\underline{r})\right|^2 \leq \mathcal{MF}(\underline{r}) \qquad \underline{r} \in \Omega \setminus \Pi(\underline{r}_t) \tag{4.2b}$$

Formulation (4.1, 4.2a-4.2b) is able to guarantee both the uniformity of the field at the target points as well as to avoid the occurrence of unwanted hot spot, by means of constrains (4.2a) and (4.2b) respectively. However, the problem is again non-linear and belonging to the class of the NP hard problems. Also, no simple trick as the one used for the focusing problem can be exploited. Luckily, as we are going to show, the problem can be recast in terms of several (different) CP problems. Assuming the field in $\underline{r}_{t1}$ to be purely real, similarly to FOCO, and exploiting the redundancy between (4.1) and (4.2a), problem (4.1, 4.2a-4.2b) can be formulated as:

For sufficiently dense sampling values of ϕ*, determine* I_n *such to:*

$$max\left\{ \Re\{E_i(\underline{r}_{t1})\} \right\} \tag{4.3}$$

subject to:

$$\Im\{E_i(\underline{r}_{t1})\} = 0 \tag{4.4a}$$

$$\Re\{E_i(\underline{r}_{t2})\} = \Re\{E_i(\underline{r}_{t1})\} cos(\phi) \qquad \phi \in [-\pi, \pi] \tag{4.4b}$$

$$\Im\{E_i(\underline{r}_{t2})\} = \Re\{E_i(\underline{r}_{t1})\} sin(\phi) \qquad \phi \in [-\pi, \pi] \tag{4.4c}$$

$$\left|\mathbf{E}(\underline{r})\right|^2 \leq \mathcal{MF}(\underline{r}) \qquad \underline{r} \in \Omega \setminus \Pi(\underline{r}_t) \tag{4.4d}$$

Where constraints (4.4b) and (4.4c) still enforce the uniformity of the field in the target points.

For any fixed value of ϕ, problem (4.3-4.3a-d) is cast as the maximization of a linear function in a convex set, which corresponds to a CP problem. As such, mt-FOCO is able to determine the globally optimal solution by solving different CP problems and then *a-posteriori* picking the most convenient one. A possible strategy, adopted in the reported results, is to select the optimal solution as the one maximizing cost function (4.1). Notably, as all the different possibilities for ϕ are explored (in a sampled fashion), one is able to guarantee the global optimality of the final excitations.

The procedure can be extended in a conceptually easy fashion to the case of more control points. Of course, a price is paid in terms of computational complexity. In fact, one will need $L-1$ (phase shifts) auxiliary variables, so that if M is the number of sampling points in each auxiliary variable, the overall number of CP problems raises as M^{L-1}. On the other side, advantages can be taken from parallel computing, as well as from non-enumerative optimization procedures for the identification of the auxiliary variables' optimal values.

It is worth of noting that comparing the proposed mt-TR with mt-FOCO, although in both one has to explore the space of "phase shifts", two relevant differences can be noted. First, at each step, just a linear superposition of fields has to be computed for mt-TR, whereas a CP problem has to be solved in mt-FOCO. Second, as it is based on a generalization/optimization of the widespread and intuitive TR technique, the mt-TR, differently from mt-FOCO, it cannot enforce any constraints on the power deposition outside the target area.

Let us also note that while a TR based technique would require sensors and applicators entirely surrounding the region of interest, the proposed approach will also work (in a provable globally optimal fashion[2]) with a restricted set of antennas (possibly covering just a part of the possible impinging directions).

Similarly to mt-TR, the approach can be extended to the case of a non-uniform shaping and the extension to the vector case can be pursued by following the guidelines implemented in [77, 78].

4.1.1 Assessment in a 3-D inhomogeneous canonical scenario

The 3-D scenario used for the validation is depicted in Fig. 4.1.(a) and consists in two dielectric objects (a cube and a sphere) hosted in free space into the cubic region of interest, i.e. Ω, of side $l \approx 2\lambda_m$[3]. The cube has a side of $l_c = \lambda_m/2$ and $\epsilon_c = 2$, whereas the sphere has a radius of $r_s = \lambda_m/4$ and $\epsilon_s = 3$. The antenna array

[2] We mean globally optimal for the given set of antennas.

[3] Being λ_m the wavelength in the background medium

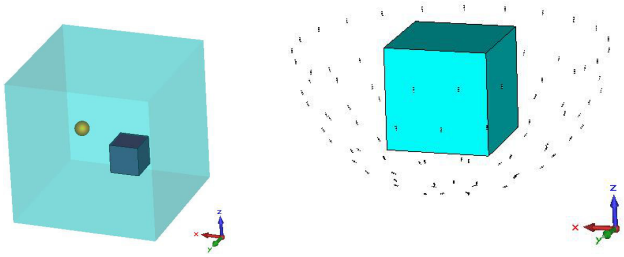

(a) (b)

Fig. 4.1. Scenario used for validation (a) and antenna array configuration (b).

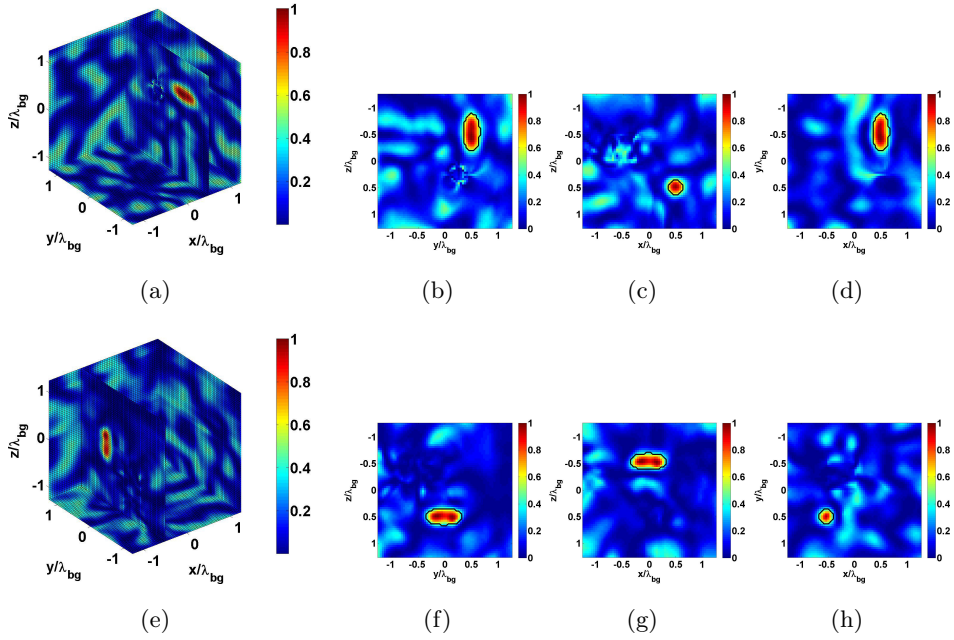

(a) (b) (c) (d)

(e) (f) (g) (h)

Fig. 4.2. Normalized shaped field intensity distribution obtained by means of mt-FOCO for both configuration respectively on a 3-D cut and on the x-, y- and z-cut view of the target area.

is an hemispherical array of radius $r \approx 4\lambda_m$ made up by 92 very small unitary-excited dipoles (i.e. approximating point-sources), arranged, along the *z-axis*, evenly distributed over 6 equi-spaced circles (23, 21, 19, 15, 9 and 5 dipoles respectively), as shown in Fig. 4.1.(b).

Full wave numerical simulations have been performed with CST Microwave STUDIO® with a working frequency of $1,5GHz$. In order to deal with a scalar field, only the *z-component* of the field has been considered. To test the reliability of the proposed approach, in this study an extended elliptical shaped target area, of axes $\approx 3\lambda_m/4 \times \lambda_m/4$, has been placed in two different positions in Ω (configurations **I** and **II** in the following).

The results, reported in Fig.4.2, have been obtained by means of the proposed mt-FOCO exploiting 2 control points evenly spaced with respect to the center of the target area and 20 values for the auxiliary variable ϕ. Fig.s 4.2.(a) and 4.2.(e) report the squared amplitude of the globally optimal solution field intensity, for configurations **I** and **II** respectively.

Note that, defining the Coverage Factor (CF) as the fraction of the target area in which $\left|\mathbf{E}(\underline{r})\right|^2$ is higher than 50% of its maximum value, the mt-FOCO allows to have CFs approximately equal to 80% and 95%, respectively for configuration **I** and **II**, while keeping the maximum side lobe level amplitude outside the target region, respectively, as low as 48% and 42%. In order to appraise the aforementioned performances of the proposed mt-FOCO, Fig.s 4.2.(b), (c), (d) and Fig.s 4.2.(f), (g), (h) report, respectively for the two configurations, three cut views along the target area.

The reported examples have been run on a workstation equipped with two Intel Xeon E5-2687W processors and 256GB RAM with a calculation time of approximately $2hrs$ each. Finally, note that no significant shaping capability of the field intensity has achieved, in both configurations (as well as in many others) by using the approach in [86].

4.1.2 Preliminary Clinical Results

In the following we present a preliminary clinical assessment of mt-FOCO on three 3-D patients models planned for treatment with the HYPERcollar3D (**A**, **B** and **C**). To effectively validate the improvement introduced by the shaping procedure, mt-FOCO has been compared to FOCO. The comparison was carried out exploiting both SAR-based and temperature-based quality metrics as reported in Appendix A. The subscripts mt-FOCO and FOCO have been added to indicate the metrics respectively related to the two optimization routines.

The control points adopted for mt-FOCO have been selected within the HTV as the centers of the minimum number of spheres of diameters $\approx \lambda_m/3$ approximating the HTV. For the considered cases, three control points have been used. On the other side, for the FOCO target point, i.e. $\underline{r}_t$, the HTV center of mass was used.

The effect of EM tissues uncertainty on mt-FOCO has been appraised by comparing the standard synthetic parameters (see Appendix A) achieved in the actual scenarios (i.e., uncertainty equal to 0%) with the ones obtained in case of uncertainty equal to $\pm 10\%$, i.e., considering a total uncertainty equal to 20%. The chosen uncertainty values have been selected accordingly with the literature [38,88]. In the work of

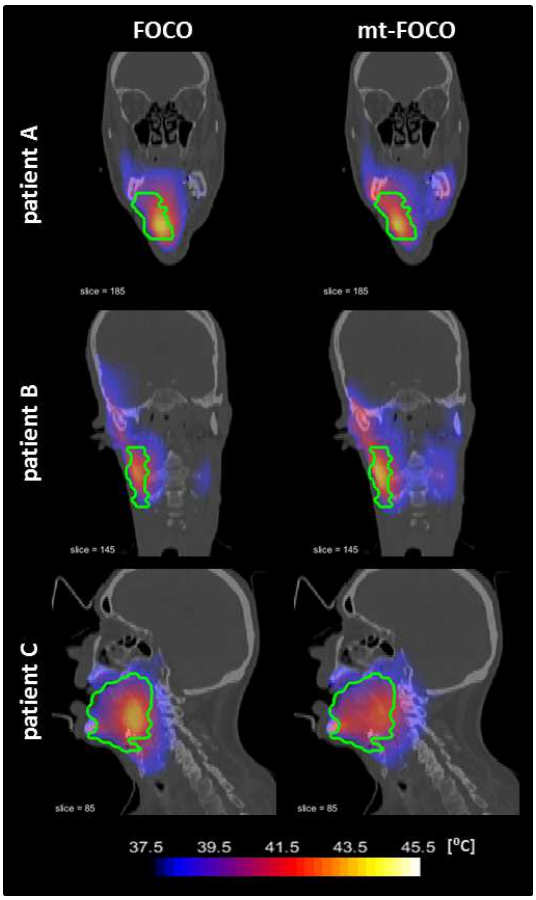

Fig. 4.3. Off center cut views of the temperature distribution obtained by means of FOCO and mt-FOCO for patient ID **A**, **B** and **C**. Target area is in green.

Table 4.1. Synthetic HTP parameters of the considered analysis

		TC25			THQ		
ID		−10%	0%	+10%	−10%	0%	+10%
A	FOCO	87	87	87	1.01	0.97	0.94
	mt-FOCO	98	99	99	1.08	1.09	1.09
B	FOCO	88	88	88	1.12	1.10	1.08
	mt-FOCO	99	99	99	1.15	1.15	1.15
C	FOCO	77	78	79	1.02	0.99	0.96
	mt-FOCO	87	88	88	1.04	1.00	0.96

Iero et.al [19], such a robustness assessment has been already carried out for FOCO bu only on 2D realistic phantoms. Hereto, we also tested the robustness of FOCO in an actual clinical setup.

Table 4.1 reports the synthetic metrics in addition to the visual information provided by Fig. 4.3. As expected, mt-FOCO outperforms the standard FOCO by an absolute % gain of $\approx$ 10-15% in terms of TC and of $\approx 5\%$ in terms of THQ, except for the challenging case **C** in which we still obtain clinically acceptable THQ values (≥ 1). The shown metrics confirm the expected robustness of the mt-FOCO when dealing with EM scenario uncertainty. The reported values differ, indeed, by a maximum of 2% for TC25 by a maximum of 7% for THQ compared to nominal situations.

The planning results have been ultimately evaluated using the temperature distribution, which is simulated using the Penne's Bio-Heat Transfer Equation [53]. The temperature distribution was achieved by adjusting SAR to a maximum of 44°C in normal tissue, i.e. outside the HTV. Figure 4.3 shows an off center cut view of the temperature distribution obtained with both FOCO and mt-FOCO for the three considered patient models. In patient **A** the T50 increases from $40,2$°C to $41,5$°C by means of FOCO and mt-FOCO, respectively. Analogously, T50 for patients **B** and **C** are increased from $39,9$°C and $40,4$°C (FOCO) to $41,0$°C and $40,5$°C (mt-FOCO), respectively. Hence, an average median temperature improvement of $\approx 0.8°C$ with respect to standard FOCO is gained by means of mt-FOCO. Note that, in 2 out of 3 patients the thermal dose is increased by a factor of 4 according to the CEM43 model [72].

Motivated by the promising results, present efforts are aimed at extending the proposed procedure to the case of vector field [77, 78].

5

Conclusion

In this thesis the problem of shaping the intensity of a (scalar) field have been considered and innovative results and approaches have been presented. Despite the very general mathematical formulation and the broad interest in many different application, this thesis was particularly focused in the planning of hyperthermia treatments. It is possible, hence, to identify a twofold interest in this thesis. First, dedicated optimization approaches with a very broad mathematical formulation and range of application were developed starting from clinical needs. Second, thanks to the collaboration with the *Hyperthermia Unit of the Department of Radiation Oncology at the Erasmus MC* (Rotterdam, The Netherlands) the approaches were tested and comparatively assessed exploiting actual patient data. This thesis represent a solid merge between theory and clinical application.

The novelties of this thesis can be briefly stated as: 1) exploitation of convex-programming based constrained algorithms in HTP [R1,R6,R10]; 2) the definition of the novel *shaping the field intensity* paradigm as opposed to "solely" focusing [R9,R11]; 3) introduction of concept borrowed from the compressive sensing for the optimal HTP [R1]. Details related to the different points are given in the following discussion.

A remarkable consideration is that, for the first time, in this thesis, planning an hyperthermia treatment has been cast as a convex programming problem. The proposed approaches, besides the one in Chapter III, are convex-programming based constrained focusing/shaping approaches [R1,R6,R10]. This opened the way to many interesting development, both theoretical and application wise. Avoiding the use of global search algorithms (as in principle) allowed the reduction of the computational time. This was shown, for instance, when comparing FOCO with the currently clinical approach adopted at Erasmus MC. From a clinical prospective, the improvement of the computational time goes towards the real-time adaptation of the administered heating, e.g., in case of patients complains. Also, in this thesis, a not very fine voxel size has been adopted to keep the computational time curbed. The circumstance of a

reduced computational time, on the other side, would allow to increase the resolution as well as a higher number of antennas at a limited increase of the computational time. Still, note that GPU implementation are feasible, hence even better performance are expected. A second main benefit related to the exploitation of a convex programming problem is that the globally optimal solution is achieved in an operator-independent fashion. This has a clear benefit into the clinical practice since (once the target point is properly set) only one solution (the globally optimal one) is delivered and no need to further adjustment are needed, as well as no (possibly arising) reproducibility issues have to be faced.

For the first time, in this thesis, the problem of shaping as opposed to focusing has been identified within the hyperthermia treatment planning framework and two different *ad-hoc* procedures have been devised and tested [R9,R11]. This problem was already known in other applications (e.g., in the telecommunication) but it wasn't properly recognized and coped in the hyperthermia framework. Still, the group of Wust et al. [55] found some optimization weakness for the larger target areas. The problem, has been tackled 1) by the adoption of more target points, named control points, rather than one target point and 2) by exploiting an additional degrees of freedom played by the phase shift of the field at the control points, so far unexploited. Firstly, in Chapter III, an un-constrained approach has been proposed [R9]. Despite the very promising results as well as the low computational burden, the impossibility of controlling undesired heating led to the development of a new optimization method. In Chapter IV, starting from the FOCO, the only constrained and convex-programming based shaping approach in the literature has been proposed and tested [R11]. Beside the interest in the methodologies, the message gathered from these investigations is that different optimization algorithms have to be used for different tumors (as well as applicator and anatomical site).

Within the hyperthermia treatment planning research, this thesis represent the creation of a novel planning tool (which has been presented in a unified mathematical framework herein). The problem of uniformly shaping the power deposition within a certain target volume in a non-homogenous media has been tackled by (five) different approaches, all of them singularly different from each other and from the state-of-the-art. The planning tool created with this thesis is made up by both focusing and shaping approaches, three and two respectively. Cornering the first category, the convex-programming based constrained focusing approach, FOCO, has been comparatively assessed against the clinical adopted optimization approach with interesting results as well as physical insight driving the present research [R6]. Secondly, for the

first time, concepts borrowed from the compressive sensing theory have been borrowed for optimally select the antennas when planning the treatment [R1]. Lastly, the physical intuition that multi-frequency applicators could eventually lead to a further reduction of the undesired heating in healthy tissues was the basis for the developed of the multi-frequency FOCO [R10]. Notably, the latter are also convex-programming based constrained focusing approaches.

Some final considerations on two important aspects which were not treated in this thesis are in the following.

Concerning the (un-constrained) method in Chapter III, note we have dealt with single frequency 3D spatial shaping (over an extended area) in loss-less media so that there has been no need to compensate for frequency dispersion and losses. In this respect, note a loss compensation technique as the ones proposed in [89–91] is needed in case of biological media. Considering both this reasoning and the strong need of controlling undesired heating in healthy tissues, we decided to propose a novel, constrained, shaping approach as reported in Chapter IV. Still, it is worth of noting that the proposed Chapter III has a very general formulation which can be eventually also generalized to the case of multi-frequency shaping by taking advantage from the concepts in Chapter II.

Finally, we have dealt with scalar fields as a step towards the optimal solution of the vector problem. Focusing or shaping the intensity of a vector field will require to merge the approach which follow with the one in [77, 78]. Hereto, an enumerative search, similar to the one proposed in Chapter III and IV, is carried out towards the determination of the optimal polarization in the target point(s). Clearly, this represents an additional computational burden which is increasing with the number of control points adopted. On the other hand, the presented approaches can be directly applied to ultrasound fields in biological media and to any case where one knows a priori that one of the field components is dominant with respect to the other ones.

A

Standard Evaluation Metrics

The SAR quality indicators used in our study are used in the clinic and implemented in VEDO. These allow understanding of the quality of the SAR distribution induced into the patient. The considered quality indicators are the target coverage and the THQ. The target coverage has been evaluated at 25%/50%/75% (TC25/TC50/TC75) level and is defined as the volume percentage of the HTV covered by 25%/50%/75% iso-SAR value when the SAR distribution is normalized to the maximum SAR in the whole patient model. As an example, TC25 equal to 50% means that the normalized SAR distribution is $\geq$0,25 in one half of the HTV. Concerning the THQ, we would refer the reader to Section 2.1.1 for a more detailed description.

A straightforward way to analyze the quality of a hyperthermia treatment is to take into account both the power deposited within the HTV and the SAR peaks outside, i.e., the so called hot-spots. As a matter of fact, the target coverage gives information on the iso-SAR level covering the HTV, i.e., within the target volume, whereas the THQ is somehow a balance of the power deposited within and outside the HTV (note, 1/THQ was also investigated in [29]). Hence, we decided to investigate these SAR quality metrics as particularly suitable and relevant for this analysis.

SAR-based indicators have been correlated to temperature-based indicators 5 being correlated to clinical outcome [16, 29, 58, 71, 72]. Those are the T50 and the T90, defined as the lower temperature covering respectively 50% or 90% of the HTV volume.

References

1. G. Lerosey, J. De Rosny, A. Tourin, A. Derode, G. Montaldo, and M. Fink, "Time reversal of electromagnetic waves and telecommunication," *Radio science*, vol. 40, no. 6, 2005.
2. T. Isernia and G. Panariello, "Optimal focusing of scalar fields subject to arbitrary upper bounds," *Electronics letters*, vol. 34, no. 2, pp. 162–164, 1998.
3. C. Larmat, J. Tromp, Q. Liu, and J.-P. Montagner, "Time reversal location of glacial earthquakes," *Journal of Geophysical Research: Solid Earth*, vol. 113, no. B9, 2008.
4. G. Micolau, M. Saillard, and P. Borderies, "Dort method as applied to ultrawideband signals for detection of buried objects," *IEEE Transactions on geoscience and remote sensing*, vol. 41, no. 8, pp. 1813–1820, 2003.
5. M. M. Paulides, G. M. Verduijn, and N. Van Holthe, "Status quo and directions in deep head and neck hyperthermia.," *Radiat Oncol*, vol. 11, no. 1, p. 21, 2016.
6. J. L. Thomas, F. Wu, and M. Fink, "Time reversal focusing applied to lithotripsy.," *Ultrasonic imaging*, vol. 18, pp. 106–121, Apr. 1996.
7. E. Zastrow *et al.*, "Time-multiplexed beamforming for noninvasive microwave hyperthermia treatment," *IEEE transactions on biomedical engineering*, vol. 58, no. 6, pp. 1574–1584, 2011.
8. R. Y. Miyamoto and T. Itoh, "Retrodirective arrays for wireless communications," *IEEE Microwave Magazine*, vol. 3, no. 1, pp. 71–79, 2002.
9. Z. Wu, R. E. Kumon, J. I. Laughner, I. R. Efimov, and C. X. Deng, "Electrophysiological changes correlated with temperature increases induced by high-intensity focused ultrasound ablation.," *Ultrasound in medicine & biology*, vol. 41, pp. 432–448, Feb. 2015.
10. L. Chen, K. Wang, Z. Chen, Z. Meng, H. Chen, H. Gao, P. Wang, H. Zhu, J. Lin, and L. Liu, "High intensity focused ultrasound ablation for patients with inoperable liver cancer.," *Hepato-gastroenterology*, vol. 62, pp. 140–143, 2015.
11. Z. Rijnen *et al.*, "Clinical integration of software tool VEDO for adaptive and quantitative application of phased array hyperthermia in the head and neck.," *Int J Hyperthermia*, vol. 29, pp. 181–193, May 2013.
12. N. R. Datta *et al.*, "Hyperthermia and radiotherapy with or without chemotherapy in locally advanced cervical cancer: a systematic review with conventional and network meta-analyses.," *International Journal of Hyperthermia*, vol. 32, pp. 809–821, Nov. 2016.

13. M. Franckena *et al.*, "Long-term improvement in treatment outcome after radiotherapy and hyperthermia in locoregionally advanced cervix cancer: an update of the Dutch Deep Hyperthermia Trial.," *Int J Radiat Oncol Biol Phys*, vol. 70, pp. 1176–1182, Mar 2008.
14. N. Cihoric *et al.*, "Hyperthermia-related clinical trials on cancer treatment within the clinicaltrials.gov registry.," *Int J Hyperthermia*, vol. 31, pp. 609–614, Sep 2015.
15. R. Issels *et al.*, "Hallmarks of hyperthermia in driving the future of clinical hyperthermia as targeted therapy: translation into clinical application.," *Int J of Hyperthermia*, vol. 32, pp. 89–95, 2016.
16. M. Sherar *et al.*, "Relationship between thermal dose and outcome in thermoradiotherapy treatments for superficial recurrences of breast cancer: data from a phase iii trial," *Int J Radiat Oncol Biol Phys*, vol. 39, no. 2, pp. 371–380, 1997.
17. P. Wust *et al.*, "Hyperthermia in combined treatment of cancer," *The Lancet Oncology*, vol. 3, no. 8, pp. 487–497, 2002.
18. P. R. Stauffer, "Evolving technology for thermal therapy of cancer.," *Int J Hyperthermia*, vol. 21, pp. 731–744, Dec 2005.
19. D. A. Iero, L. Crocco, and T. Isernia, "Thermal and microwave constrained focusing for patient-specific breast cancer hyperthermia: A robustness assessment," *IEEE Transactions on Antennas and Propagation*, vol. 62, no. 2, pp. 814–821, 2014.
20. M. M. Paulides *et al.*, "Simulation techniques in hyperthermia treatment planning.," *Int J Hyperthermia*, vol. 29, pp. 346–357, Jun 2013.
21. H. Kok *et al.*, "High-resolution temperature-based optimization for hyperthermia treatment planning," *Physics in Medicine & Biology*, vol. 50, no. 13, p. 3127, 2005.
22. H. Lee, A. Antell, *et al.*, "Superficial hyperthermia and irradiation for recurrent breast carcinoma of the chest wall: Prognostic factors in 196 tumors," *Int J Radiat Oncol Biol Phys*, vol. 40, pp. 365–75, 1998.
23. D. H. Wolpert and W. G. Macready, "No free lunch theorems for optimization," *IEEE Transactions on Evolutionary Computation*, vol. 1, pp. 67–82, Apr. 1997.
24. M. Seebass, R. Beck, J. Gellermann, J. Nadobny, and P. Wust, "Electromagnetic phased arrays for regional hyperthermia: optimal frequency and antenna arrangement.," *International journal of hyperthermia : the official journal of European Society for Hyperthermic Oncology, North American Hyperthermia Group*, vol. 17, pp. 321–336, 2001.
25. J. Gellermann, M. Weihrauch, C. H. Cho, W. Wlodarczyk, H. Fähling, R. Felix, V. Budach, M. Weiser, J. Nadobny, and P. Wust, "Comparison of mr-thermography and planning calculations in phantoms.," *Medical physics*, vol. 33, pp. 3912–3920, Oct. 2006.
26. T. Köhler, P. Maass, P. Wust, and M. Seebass, "A fast algorithm to find optimal controls of multiantenna applicators in regional hyperthermia.," *Physics in medicine and biology*, vol. 46, pp. 2503–2514, Sept. 2001.
27. R. A. M. Canters *et al.*, "Benefit of replacing the sigma-60 by the sigma-eye applicator. a monte carlo-based uncertainty analysis.," *Strahlenther Onkol*, vol. 189, pp. 74–80, Jan 2013.

28. C. W. Song, "Effect of local hyperthermia on blood flow and microenvironment: A review," *Cancer Research*, vol. 44, no. 10 Supplement, pp. 4721s–4730s, 1984.

29. R. A. M. Canters *et al.*, "A literature survey on indicators for characterisation and optimisation of SAR distributions in deep hyperthermia, a plea for standardisation.," *Int J Hyperthermia*, vol. 25, pp. 593–608, Nov 2009.

30. M. De Greef, H. Kok, D. Correia, A. Bel, and J. Crezee, "Optimization in hyperthermia treatment planning: the impact of tissue perfusion uncertainty," *Medical physics*, vol. 37, no. 9, pp. 4540–4550, 2010.

31. M. de Greef, H. P. Kok, D. Correia, P.-P. Borsboom, A. Bel, and J. Crezee, "Uncertainty in hyperthermia treatment planning: the need for robust system design.," *Physics in medicine and biology*, vol. 56, pp. 3233–3250, June 2011.

32. G. Cappiello *et al.*, "Differential evolution optimization of the sar distribution for head and neck hyperthermia.," *IEEE transactions on bio-medical engineering*, vol. 64, pp. 1875–1885, Aug. 2017.

33. Z. Rijnen *et al.*, "Quality and comfort in head and neck hyperthermia: A redesign according to clinical experience and simulation studies.," *Int J Hyperthermia*, pp. 1–8, Oct 2015.

34. E. Zastrow, S. C. Hagness, B. D. V. Veen, and J. E. Medow, "Time-multiplexed beamforming for noninvasive microwave hyperthermia treatment," *IEEE Transactions on Biomedical Engineering*, vol. 58, pp. 1574–1584, June 2011.

35. M. Tanter *et al.*, "Optimal focusing by spatio-temporal inverse filter. i. basic principles," *The Journal of the Acoustical Society of America*, vol. 110, no. 1, pp. 37–47, 2001.

36. P. Takook *et al.*, "A computational study using time reversal focusing for hyperthermia treatment planning," *Progress In Electromagnetics Research*, vol. 73, pp. 117–130, 2017.

37. M. Fink, "Time reversal of ultrasonic fields. i. basic principles," *IEEE transactions on ultrasonics, ferroelectrics, and frequency control*, vol. 39, no. 5, pp. 555–566, 1992.

38. V. Fortunati *et al.*, "Tissue segmentation of head and neck ct images for treatment planning: A multiatlas approach combined with intensity modeling.," *Med Phys*, vol. 40, p. 071905, Jul 2013.

39. R. F. Verhaart *et al.*, "Accurate 3D temperature dosimetry during hyperthermia therapy by combining invasive measurements and patient-specific simulations.," *Int J Hyperthermia*, vol. 31, pp. 686–692, Sep 2015.

40. P. Togni *et al.*, "Electromagnetic redesign of the hypercollar applicator: toward improved deep local head-and-neck hyperthermia.," *Phys Med Biol*, vol. 58, pp. 5997–6009, Sep 2013.

41. H. P. Kok, M. D. Greef, N. V. Wieringen, D. Correia, M. C. C. M. Hulshof, P. J. Zum, J. Sijbrands, A. Bel, and J. Crezee, "Comparison of two different 70 MHz applicators for large extremity lesions: simulation and application.," *Int J Hyperthermia*, vol. 26, no. 4, pp. 376–388, 2010.

42. H. Dobsek Trefna, J. Vrba, and M. Persson, "Evaluation of a patch antenna applicator for time reversal hyperthemia.," *International journal of hyperthermia : the official journal*

of European Society for Hyperthermic Oncology, North American Hyperthermia Group, vol. 26, pp. 185–197, 2010.

43. P. Takook, M. Persson, J. Gellermann, and H. D. TrefnÃ¡, "Compact self-grounded bow-tie antenna design for an uwb phased-array hyperthermia applicator.," *International journal of hyperthermia : the official journal of European Society for Hyperthermic Oncology, North American Hyperthermia Group*, pp. 1–14, Jan. 2017.
44. L. Winter, C. Özerdem, W. Hoffmann, D. Santoro, A. Müller, H. Waiczies, R. Seemann, A. Graessl, P. Wust, and T. Niendorf, "Design and evaluation of a hybrid radiofrequency applicator for magnetic resonance imaging and rf induced hyperthermia: electromagnetic field simulations up to 14.0 tesla and proof-of-concept at 7.0 tesla.," *PloS one*, vol. 8, p. e61661, 2013.
45. T. Niendorf, C. Oezerdem, Y. Ji, E. Oberacker, A. Kuehne, H. Waiczies, and L. Winter, "Radiative RF antenna arrays for cardiac, brain and thermal magnetic resonance at ultrahigh and extreme magnetic field strengths: Concepts, electromagnetic field simulations and applications," in *Proc. Int. Conf. Electromagnetics in Advanced Applications (ICEAA)*, pp. 1567–1570, Sept. 2017.
46. J. J. Liang and P. N. Suganthan, "Dynamic multi-swarm particle swarm optimizer," in *Proc. IEEE Swarm Intelligence Symp. SIS 2005*, pp. 124–129, June 2005.
47. A. Miranda, T. Cova, J. Sousa, C. Vitorino, and A. Pais, "Computational modeling in glioblastoma: from the prediction of blood-brain barrier permeability to the simulation of tumor behavior.," *Future medicinal chemistry*, vol. 10, pp. 121–131, Jan. 2018.
48. E. K. Noch, R. Ramakrishna, and R. Magge, "Challenges in the treatment of glioblastoma: Multisystem mechanisms of therapeutic resistance.," *World neurosurgery*, vol. 116, pp. 505–517, Aug. 2018.
49. E. J. Candès *et al.*, "Compressive sampling," in *Proceedings of the international congress of mathematicians*, vol. 3, pp. 1433–1452, Madrid, Spain, 2006.
50. N. Burnet, S. Thomas, K. Burton, and S. Jefferies, "Defining the tumour and target volumes for radiotherapy," *Cancer Imaging*, no. 4(2), pp. 153–161, 2004.
51. M. M. Paulides *et al.*, "Assessment of the local SAR distortion by major anatomical structures in a cylindrical neck phantom.," *Int J Hyperthermia*, vol. 21, pp. 125–140, Mar 2005.
52. O. M. Bucci, C. Gennarelli, and C. Savarese, "Representation of electromagnetic fields over arbitrary surfaces by a finite and nonredundant number of samples," *IEEE Transactions on Antennas and Propagation*, vol. 46, pp. 351–359, Mar. 1998.
53. H. H. Pennes, "Analysis of tissue and arterial blood temperatures in the resting human forearm.," *J Appl Physiol*, vol. 1, pp. 93–122, Aug 1948.
54. L. R. Dice, "Measures of the amount of ecologic association between species," *Ecology*, 1945.
55. P. Wust, M. Seebass, J. Nadobny, P. Deuflhard, G. Mönich, and R. Felix, "Simulation studies promote technological development of radiofrequency phased array hyperther-

mia.," *International journal of hyperthermia : the official journal of European Society for Hyperthermic Oncology, North American Hyperthermia Group*, vol. 12, pp. 477–494, 1996.

56. T. Drizdal *et al.*, "Hyperthermia treatment planning guided applicator selection for subsuperficial head and neck tumors heating," *Int J Hyperthermia*, vol. 0, no. ja, pp. 1–28, 2017. PMID: 28931333.
57. H. P. Kok, L. Korshuize-van Straten, A. Bakker, R. de Kroon-Oldenhof, E. D. Geijsen, L. J. A. Stalpers, and J. Crezee, "Online adaptive hyperthermia treatment planning during locoregional heating to suppress treatment-limiting hot spots.," *International journal of radiation oncology, biology, physics*, vol. 99, pp. 1039–1047, Nov. 2017.
58. D. E. Thrall *et al.*, "Using units of CEM 43C T90, local hyperthermia thermal dose can be delivered as prescribed," *International Journal of Hyperthermia*, vol. 16, no. 5, 2000.
59. M. Franckena *et al.*, "Hyperthermia dose-effect relationship in 420 patients with cervical cancer treated with combined radiotherapy and hyperthermia.," *Eur J Cancer*, vol. 45, pp. 1969–1978, Jul 2009.
60. G. Bruggmoser *et al.*, "Guideline for the clinical application, documentation and analysis of clinical studies for regional deep hyperthermia Quality management in regional deep hyperthermia," *Strahlentherapie und Onkologie*, vol. 188, no. 2, pp. 198–211, 2012.
61. M. M. Paulides, R. M. C. Mestrom, G. Salim, B. B. Adela, W. C. M. Numan, T. Drizdal, D. T. B. Yeo, and A. B. Smolders, "A printed yagi-uda antenna for application in magnetic resonance thermometry guided microwave hyperthermia applicators.," *Physics in medicine and biology*, vol. 62, pp. 1831–1847, Mar. 2017.
62. W. C. M. Numan, L. W. Hofstetter, G. Kotek, J. F. Bakker, E. W. Fiveland, G. C. Houston, G. Kudielka, D. T. B. Yeo, and M. M. Paulides, "Exploration of mr-guided head and neck hyperthermia by phantom testing of a modified prototype applicator for use with proton resonance frequency shift thermometry.," *Int J Hyperthermia*, vol. 30, pp. 184–191, May 2014.
63. D. A. M. Iero, L. Crocco, and T. Isernia, "Design of biomedical array applicators: An innovative constrained synthesis strategy to focusing vector fields," in *Proc. 1st URSI Atlantic Radio Science Conf. (URSI AT-RASC)*, p. 1, May 2015.
64. O. M. Bucci and T. Isernia, "Electromagnetic inverse scattering: Retrievable information and measurement strategies," *Radio Science*, vol. 32, pp. 2123–2137, Nov. 1997.
65. O. M. Bucci, L. Crocco, R. Scapaticci, and G. Bellizzi, "On the design of phased arrays for medical applications," *Proceedings of the IEEE*, vol. 104, pp. 633–648, Mar. 2016.
66. D. L. Donoho, "Compressed sensing," *IEEE Transactions on information theory*, vol. 52, no. 4, pp. 1289–1306, 2006.
67. T. Blumensath, M. Yaghoobi, and M. E. Davies, "Iterative hard thresholding and l0 regularisation," in *Proc. IEEE Int. Conf. Acoustics Speech and Signal Processing - ICASSP '07*, vol. 3, pp. III–877–III–880, Apr. 2007.

68. X. Chen, Z. J. Wang, and M. J. McKeown, "Fmri group studies of brain connectivity via a group robust lasso," in *Proc. IEEE Int. Conf. Image Processing*, pp. 589–592, Sept. 2010.

69. J. A. Bazerque, G. Mateos, and G. B. Giannakis, "Distributed lasso for in-network linear regression," in *Proc. Speech and Signal Processing 2010 IEEE Int. Conf. Acoustics*, pp. 2978–2981, Mar. 2010.

70. G. G. Bellizzi *et al.*, "Do sar quality indicators predict temperature? a verification study in head and neck hyperthermia," in *STRAHLENTHERAPIE UND ONKOLOGIE*, vol. 194, pp. 504–505.

71. M. de Bruijne, B. van der Holt, G. C. van Rhoon, and J. van der Zee, "Evaluation of CEM43 degrees CT90 thermal dose in superficial hyperthermia: a retrospective analysis.," *Strahlenther Onkol*, vol. 186, pp. 436–443, Aug 2010.

72. G. C. van Rhoon, "Is cem43 still a relevant thermal dose parameter for hyperthermia treatment monitoring?," *International journal of hyperthermia : the official journal of European Society for Hyperthermic Oncology, North American Hyperthermia Group*, vol. 32, pp. 50–62, 2016.

73. D. L. Donoho, "For most large underdetermined systems of linear equations the minimal ?1-norm solution is also the sparsest solution," *Communications on Pure and Applied Mathematics: A Journal Issued by the Courant Institute of Mathematical Sciences*, vol. 59, no. 6, pp. 797–829, 2006.

74. G. G. Bellizzi, T. Drizdal, G. C. van Rhoon, T. Crocco, Lorenzoand Isernia, and M. M. Paulides, "The potential of constrained SAR focusing for hyperthermia treatment planning: analysis for the head & neck region," *Physics in Medicine and Biology*, 2018.

75. H. D. Trefna, J. P. de Berrazueta, and M. Persson, "Experimental verification of time-reversal microwave hyperthermia system," in *Proc. XXXth URSI General Assembly and Scientific Symp*, pp. 1–3, Aug. 2011.

76. H. D. Trefna, B. Martinsson, T. Petersson, N. Renstrom, M. Torstensson, J. Ravanis, P. Kok, and M. Persson, "Multifrequency approach in hyperthermia treatment planning: Impact of frequency on SAR distribution in head and neck," in *Proc. 11th European Conf. Antennas and Propagation (EUCAP)*, pp. 3710–3712, Mar. 2017.

77. D. A. M. Iero, "Constrained power focusing in inhomogeneous media as a polarization optimization," *International Journal of Antennas and Propagation*, vol. 2015, 2015.

78. D. A. Iero, L. Crocco, and T. Isernia, "On the role and choice of source polarization in time-reversal focusing of vector fields," *IEEE Antennas and Wireless Propagation Letters*, vol. 15, pp. 214–217, 2016.

79. E. Z. *, S. K. Davis, M. Lazebnik, F. Kelcz, B. D. V. Veen, and S. C. Hagness, "Development of anatomically realistic numerical breast phantoms with accurate dielectric properties for modeling microwave interactions with the human breast," *IEEE Transactions on Biomedical Engineering*, vol. 55, pp. 2792–2800, Dec. 2008.

80. S. Gabriel, R. W. Lau, and C. Gabriel, "The dielectric properties of biological tissues: III. Parametric models for the dielectric spectrum of tissues.," *Phys Med Biol*, vol. 41, pp. 2271–2293, Nov 1996.

81. I. Catapano, L. Crocco, M. D'Urso, A. Morabito, and T. Isernia, "Microwave tomography of breast cancer: A feasibility study," in *Proc. First European Conf. Antennas and Propagation*, pp. 1–5, Nov. 2006.

82. I. Catapano, L. Crocco, L. D. Donato, G. Angiulli, T. Isernia, A. Morabito, S. Tringali, and O. M. Bucci, "Guidelines for effective microwave breast imaging: A numerical assessment against 3D anthropomorphic phantoms," in *Proc. Fourth European Conf. Antennas and Propagation*, pp. 1–5, Apr. 2010.

83. M. Converse, E. J. Bond, B. D. Veen, and C. Hagness, "A computational study of ultra-wideband versus narrowband microwave hyperthermia for breast cancer treatment," *IEEE Transactions on Microwave Theory and Techniques*, vol. 54, pp. 2169–2180, May 2006.

84. A. Luini, G. Gatti, S. Zurrida, N. Talakhadze, F. Brenelli, D. Gilardi, G. Paganelli, R. Orecchia, E. Cassano, G. Viale, C. Sangalli, B. Ballardini, G. R. dos Santos, and U. Veronesi, "The evolution of the conservative approach to breast cancer.," *Breast (Edinburgh, Scotland)*, vol. 16, pp. 120–129, Apr. 2007.

85. A. Luini, J. Rososchansky, G. Gatti, S. Zurrida, P. Caldarella, G. Viale, G. Rosali dos Santos, and A. Frasson, "The surgical margin status after breast-conserving surgery: discussion of an open issue.," *Breast cancer research and treatment*, vol. 113, pp. 397–402, Jan. 2009.

86. D. Zhao, "Shaping microwave field of arbitrary intensity patterns in bounded area by time reversal mirror," in *Proc. Progress in Electromagnetic Research Symp. (PIERS)*, p. 4428, Aug. 2016.

87. M. M. Paulides, S. H. J. A. Vossen, A. P. M. Zwamborn, and G. C. van Rhoon, "Theoretical investigation into the feasibility to deposit RF energy centrally in the head-and-neck region.," *Int J Radiat Oncol Biol Phys*, vol. 63, pp. 634–642, Oct 2005.

88. R. F. Verhaart, V. Fortunati, G. M. Verduijn, A. van der Lugt, T. van Walsum, J. F. Veenland, and M. M. Paulides, "The relevance of mri for patient modeling in head and neck hyperthermia treatment planning: a comparison of ct and ct-mri based tissue segmentation on simulated temperature.," *Med Phys*, vol. 41, p. 123302, Dec 2014.

89. P. Kosmas, "Application of the dort technique to FDTD-based time reversal for microwave breast cancer detection," in *Proc. European Microwave Conf*, pp. 306–308, Oct. 2007.

90. M. Tanter, J.-L. Thomas, and M. Fink, "Focusing and steering through absorbing and aberrating layers: Application to ultrasonic propagation through the skull," *The Journal of the Acoustical Society of America*, vol. 103, no. 5, pp. 2403–2410, 1998.

91. M. E. Yavuz, *Time reversal based signal processing techniques for ultrawideband electromagnetic sensing in random media*. PhD thesis, The Ohio State University, 2007.

Publications

Journal Papers

R1 Gennaro G. Bellizzi, M. M. Paulides, T. Drizdal, G. C. van Rhoon, L. Crocco and T. Isernia, Selecting the Optimal Subset of Antennas in Hyperthermia Treatment Planning, IEEE Jour. of EM, RF in Med. and Bio., *Under Review*

R2 Gennaro G. Bellizzi and M. T. Bevacqua, The Linear Sampling Method as a Tool for "Blind" Field Intensity Shaping, IEEE Trans. Ant. Prop., *Under Review*

R3 G. M. Battaglia, Gennaro G. Bellizzi, A. F. Morabito, G. Sorbello, T. Isernia, Optimal Synthesis of Shaped Beams for Generic Fixed Geometry Arrays, IEEE Trans. Ant. Prop., *Under Review*

R4 Gennaro G. Bellizzi, T. Drizdal, G. C. van Rhoon, L. Crocco, T. Isernia and M. M. Paulides, Predictive Value of SAR Based Quality Indicators for Head and Neck Hyperthermia Treatment Quality, International Journal of Hyperthermia, In Press

R5 M. T. Bevacqua, Gennaro G. Bellizzi, L. Crocco and T. Isernia, A Method for Quantitative Imaging of Electrical Properties of Human Tissues from Only Amplitude Electromagnetic Data, Inverse Problems, In Press

R6 Gennaro G. Bellizzi, T. Drizdal, G. C. van Rhoon, L. Crocco, T. Isernia and M. M. Paulides, The Potential of Constrained SAR Focusing for Hyperthermia Treatment Planning: Analysis for the Head&Neck Region, Phy. in Med. and Bio., In Press

R7 M. T. Bevacqua, Gennaro G. Bellizzi, T. Isernia, L. Crocco, A Method for Effective Permittivity and Conductivity Mapping of Biological Scenarios via Segmented Contrast Source Inversion, Progress In Electromagnetics Research, Vol. 164, 1-15, 2019

R8 F. G. Della Corte, M. Merenda, Gennaro G. Bellizzi, T. Isernia, R. Carotenuto, Temperature Effects on the Efficiency of Dickson Charge Pumps for Radio Frequency Energy Harvesting, IEEE Access, In press

R9 Gennaro G. Bellizzi, M. T. Bevacqua, L. Crocco, T. Isernia, Optimized Multi-Target Time Reversal for 3-D Field Intensity Shaping, IEEE Trans. Ant. Prop., vol. 66, is. 8, pp. 4380-4385, August 2018;

R10 Gennaro G. Bellizzi, G. M. Battaglia, L. Crocco, T. Isernia, Multi-Frequency Constrained SAR Focusing for Patient Specific Hyperthermia Treatment, IEEE Jour. of EM, RF in Med. and Bio., vol. 1, is. 2, pp. 74-80, Dec. 2017

R11 Gennaro G. Bellizzi, D.A.M. Iero, L. Crocco, T. Isernia, Three-Dimensional Field Intensity Shaping: The Scalar Case, IEEE Antennas and Wireless Propagation Letters, vol. 17, is. 3, pp. 360-363, March 2018;

R12 R. Scapaticci, Gennaro G. Bellizzi, M. Cavagnaro, L. Crocco, V. Lopresto, Microwave Thermal Ablation Monitoring Via Microwave Tomography, Int. Jour. of Ant. and Prop., Oct. 2017; DOI: 10.1155/2017/5231065

R13 G. Bellizzi, Gennaro G. Bellizzi, O. M. Bucci, L. Crocco, M. Helbig, S. Ley, J. Sachs, Optimization of The Working Conditions For Magneticnanoparticle-Enhanced Microwave Diagnostics of Breast Cancer, IEEE Trans. on Biom. Eng., vol. 7, is. 7, pp. 1607-1616, July 2018;

R14 O. M. Bucci, G. Bellizzi, Gennaro G. Bellizzi, Microwave Broadband Characterization of a Diluted Water-Based Ferrofluid In Presence of A Polarizing Magnetic Field, IEEE Trans. on Magnetic, vol. 53, Is. 3, March 2017.

Conference Proceedings

C1 Gennaro G. Bellizzi, M.M. Paulides, T. Drizdal, G.C. van Rhoon, L. Crocco, T. Isernia, Sparsity Promoted Antenna Selection in Hyperthermia Treatment Planning, 1st EMF-Med World Conference on Biomedical Applications of Electromagnetic Fields, Split, Croatia, September 2018.

C2 M. T. Bevacqua, Gennaro G. Bellizzi, L. Crocco, T. Isernia, In-Vivo Mapping of Human Tissues from Only Amplitude Electromagnetic Data, 1st EMF-Med World Conference on Biomedical Applications of Electromagnetic Fields, Split, Croatia, September 2018.

C3 Gennaro G. Bellizzi, T. Drizdal, G.C. van Rhoon, L. Crocco, T. Isernia, M.M. Paulides, Do SAR Quality Indicators predict Temperature? A Verification Study in Head and Neck Hyperthermia, STRAHLENTHERAPIE UND ONKOLOGIE 194 (5), 504-505

C4 Gennaro G. Bellizzi, T. Drizdal, G.C. van Rhoon, L. Crocco, T. Isernia, M.M. Paulides, Advances in multi-target FOCO for Hyperthermia Treatment Planning: A Robustness Assessment, EuCAP, London, England, April 2018.

C5 Gennaro G. Bellizzi, T. Drizdal, G.C. van Rhoon, L. Crocco, T. Isernia, M.M. Paulides, Advances in multi-target FOCO for Hyperthermia Treatment Planning: A Robustness Assessment, EuCAP, London, England, April 2018.

C6 R. Scapaticci, Gennaro G. Bellizzi, M. Cavagnaro, V. Lopresto, R. Pinto, L. Crocco, Towards an Experimental Validation of Microwave Imaging Monitored Ablation Treatments , EuCAP, London, England, April 2018.

C7 M. T. Bevacqua, Gennaro G. Bellizzi, L. Crocco, T. Isernia, New In-vivo Estimation of Electrical Properties of Biological Tissues for Hyperthermia Treatment Planning , EuCAP, London, England, April 2018.

C8 Gennaro G. Bellizzi, L. Crocco, T. Isernia, Spatial Field Intensity Shaping via Optimized multi target Time Reversal, 32nd URSI GASS, Montreal, Canada, August, 2017.

C9 T. Isernia, Gennaro G. Bellizzi, L. Crocco, Multi-Frequency SAR Constrained Focusing for Hyperthermia Treatment Planning, ICEAA, Verona, Italia, September, 2017.

C10 Gennaro G. Bellizzi, L. Crocco, T. Isernia SAR Constrained Focusing Through Multi-Frequency Array Applicators, International Microwave Bio Conference, Göteborg, Sweden, May, 2017.

C11 D. A.M. Iero, Gennaro G. Bellizzi, T. Isernia, L. Crocco, Towards 3D Field Intensity Shaping for Biomedical Applications, EuCAP, Paris, France, March, 2017.

C12 Gennaro G. Bellizzi, L. Crocco, M. Cavagnaro, L. Farina, V. Lopresto, R. Scapaticci, A Full-Wave Numerical Assessment of Microwave Tomography for Monitoring Cancer Ablation, EuCAP, Paris, France, March 2017.

C13 Gennaro G. Bellizzi, L. Crocco, D. A.M. Iero, T. Isernia, Arbitrary Field Intensity Shaping via Multi-Target Optimal Constrained Power Focusing, IWAT, Athens, Greece, March 2017.

C14 G. Bellizzi, Gennaro G. Bellizzi, O. M. Bucci, Wideband Characterization of a Diluted Water Ferrofluid in Presence of a Polarizing Magnetic Field for Application in Biomedicine, EuCAP, Paris, March, 2017.

C15 G. Bellizzi, Gennaro G. Bellizzi, O.M. Bucci, Microwave Characterization of a diluted Water-Based Ferrofluid in presence of an External Polarizing Magnetic Field for Biomedical Applications, RinEM, Parma, Italy, September 2016.

C16 R. Scapaticci, Gennaro G. Bellizzi, O.M. Bucci, M. Cavagnaro, L. Crocco, V. Lopresto, Feasibility Study on the Use of the Microwave on the use of Microwave Tomography for Temperature Monitoring in Ablation Treatments, RinEM, Parma, Italy, September 2016.

C17 G. Bellizzi, Gennaro G. Bellizzi, O. M. Bucci, A Full-Wave Numerical Study to Investigate the Possibility of Using Microwaves for Image-Monitored Ablation Treatments, BioEMS, Gant, Belgium, May 2016.

C18 G. Bellizzi, Gennaro G. Bellizzi, O.M. Bucci, Optimization of Working Conditions for Magnetic Nanoparticle Enhanced Ultra-Wide Band Breast Cancer Detection, EuCAP, Davos, Switzerland, April 2016.

C19 Gennaro G. Bellizzi, G. Bellizzi, O. M. Bucci, L. Crocco, M. Helbig, S. Ley, J. Sachs, Optimization of Working Conditions for Magnetic Nanoparticle Enhanced Ultra-Wide Band Breast Cancer Detection, EuCAP, Davos, Switzerland, April 2016.